Master's thesis

NTNU
Norwegian University of Science and Technology
Faculty of Information Technology and Electrical Engineering
Department of Engineering Cybernetics

Jonas Anker Horntvedt

Automated docking for underactuated surface vessels: A docking-adapter assisted approach

Master's thesis in Cybernetics and Robotics
Supervisor: Tor Arne Johansen
Co-supervisor: Emil Hjelseth Thyri
June 2023

NTNU
Norwegian University of
Science and Technology

Jonas Anker Horntvedt

Automated docking for underactuated surface vessels: A docking-adapter assisted approach

Master's thesis in Cybernetics and Robotics
Supervisor: Tor Arne Johansen
Co-supervisor: Emil Hjelseth Thyri
June 2023

Norwegian University of Science and Technology
Faculty of Information Technology and Electrical Engineering
Department of Engineering Cybernetics

NTNU
Norwegian University of
Science and Technology

Summary

When designing autonomous vessels for dock-to-dock operation, automating every aspect of the journey is crucial. The dock-to-dock operation typically comprises three phases: undocking, transit, and docking. Undocking involves the vessel leaving the dock, transit refers to the vessel's movement between docking areas, and docking entails the vessel aligning with the pier. Unmanned Surface Vessels (USVs) can be categorized into fully actuated and underactuated vessels. Fully actuated vessels can move in every degree of freedom independently, whereas underactuated vessels typically only possess the ability to rotate and move forwards. Underactuated USVs may be utilized for cost-effectiveness, requiring fewer actuators or integrating older boats with autonomous capabilities.

This Master's thesis presents a comprehensive plan for the dock-to-dock process of an underactuated USV, with a specific emphasis on the docking procedure. In this docking sequence, a docking adapter similar to the ones utilized by river shuttles in Paris is employed. The USV is equipped with a docking hitch, while the pier is fitted with a docking receiver. The primary objective of the docking sequence is to securely connect the docking hitch with the receiver and subsequently align the vessel with the pier. The vessel will rotate to initiate the undocking sequence while the docking adapters are still attached, followed by reversing away from the pier. The traditional Line-of-Sight (LOS) guidance method is utilized during the transit phase.

The docking sequence comprises several stages: approach turning point, turn, approach docking, and docking rotation. Upon entering the docking area, the docking phase commences with the vessel's approach to the turning point. In cases where docking areas are limited in size, the vessel executes a turn at a designated point to ensure entry into the docking receiver from the correct side. After completing the turn and aligning itself with the docking receiver, the vessel approaches the docking receiver. Once the docking hitch is mated with the receiver, the vessel rotates its aft toward the pier to get the vessel aligned with the pier.

A simulation environment has been created for replicating the three distinct stages of the dock-to-dock operation. The simulator area represents a pier featuring a docking receiver. A vessel resembling Maritime Robotics' USV Otter is utilized within the simulation, complete with a docking hitch. This vessel is a compact catamaran equipped with two fixed thrusters positioned at the rear of each hull.

The undocking and transit stages were subjected to testing in the simulation environment under a wind speed of 7m/s, covering all wind directions from -180° to 180° with 25° increments. In all scenarios, both the undocking and transit processes were accomplished successfully.

The docking procedure underwent more extensive testing compared to the undocking and transit stages in order to ensure its effectiveness and reliability. Like the undocking and transit stages, the docking process was assessed for various wind directions spanning from -180° to 180°. However, additional tests were conducted by varying the wind speeds from 0 to 7m/s in increments of 0.1m/s. The simulation demonstrated that the USV could successfully dock under all tested conditions, but during the most challenging wind condition, the operation was not as tightly controlled. In such instances, the scheme required larger error margins. Nevertheless, under average circumstances, the docking scheme exhibited favorable outcomes and ensured a safe and controlled docking process.

Sammendrag

Når man designer autonome fartøy for dokk-til-dokk-operasjoner, er det avgjørende å automatisere alle aspekter av reisen. Dokk-til-dokk-operasjonen består typisk av tre faser: frakobling, transport og dokking. Frakobling innebærer at fartøyet forlater kaia, transport refererer til fartøyets bevegelse mellom dokkområder, og dokking innebærer at fartøyet legger til kai. Ubemannede overflatefartøy (USV-er) kan kategoriseres som fullt aktuerte og underaktuerte fartøy. Fullt aktuerte fartøy kan bevege seg uavhengig i alle frihetsgrader, mens underaktuerte fartøy typisk bare har evnen til å rotere og bevege seg framover. Underaktuerte USV-er er aktuelle ettersom de kan være kostnadseffektive, da de krever færre aktuatorer eller når eldre båter skal integreres med autonome egenskaper.

Denne masteroppgaven presenterer en omfattende plan for dokk-til-dokk-prosessen til en underaktuert USV, med spesiell vekt på dokking-prosedyren. I denne dokkingsekvensen brukes en dokkingsadapter lik de som brukes av elveferger i Paris. USV-en er utstyrt med en dokkekrok, mens kaikanten er utstyrt med en dokkingsmottaker. Det primære målet med dokkingsekvensen er å sikre en trygg tilkobling mellom dokkekroken og mottakeren, og deretter justere fartøyet med kaikanten. Fartøyet vil rotere for å starte frakoblingssekvensen mens dokkingsadapterne fortsatt er festet, etterfulgt av å reversere vekk fra kaikanten. Den tradisjonelle siktelinjemetoden (LOS) brukes under transportfasen.

Dokkingsekvensen består av flere trinn: tilnærming til snupunkt, snu, tilnærming til dokking og dokkingrotasjon. Når fartøyet kommer inn i dokkområdet, begynner dokkingfasen med fartøyets tilnærming til snupunktet. I tilfeller der dokkområdene er begrenset i størrelse, utfører fartøyet en sving på et angitt punkt for å sikre inngang til dokkingsmottakeren fra riktig side. Etter å ha fullført svingen og justert seg med dokkingsmottakeren, nærmer fartøyet seg dokkingsmottakeren. Når dokkekroken er tilkoblet mottakeren, roterer akteret på fartøyet mot kaikanten for å justere fartøyet med kaikanten.

Det er opprettet et simuleringmiljø for å gjenskape de tre ulike aspektene ved dokk-til-dokk-operasjonen. Simulatorområdet representerer en brygge med en dokkingsmottaker. Et en modell av Maritime Robotics' USV Otter blir brukt i simuleringen, komplett med en dokkingkrok. Dette fartøyet er en kompakt katamaran utstyrt med to faste thrusters plassert på baksiden av hver skrogdel.

Frakobling- og transport-stadiene ble testet i simuleringen med en vindhastighet på 7m/s, og dekket alle vindretninger fra -180° til 180° med 25° intervaller. I alle scenarioene ble både frakobling- og transport-prosessene gjennomført suksessfullt.

Dokkingsprosedyren ble utsatt for mer omfattende testing sammenlignet med frakobling- og transport-stadiene for å sikre effektivitet og pålitelighet. Som i frakobling- og transport-stadiene ble dokkingsprosessen vurdert for ulike vindretninger som spenner fra -180° til

180°. Imidlertid ble det gjennomført ekstra tester ved å variere vindhastighetene fra 0 til 7m/s med intervaller på 0.1m/s. Simuleringen viste at USV-en kunne dokke suksessfullt under alle testede forhold, men under de mest utfordrende vindforholdene var ikke operasjonen like godt kontrollert. I slike tilfeller kreves det større feilmarginer. Likevel viste dokkingsprosedyren gode resultater og sikret en trygg og kontrollert dokkingsprosess under gjennomsnittlige forhold.

Preface

I am submitting this thesis as a mandatory component for the completion of the Master's thesis TTK4900. Throughout the period of fall 2022 and spring 2023, I had the privilege of engaging in research on docking for underactuated vessels at the Department of Engineering Cybernetics, NTNU in Trondheim. In the fall semester, the work carried out was presented as a specialization project, and certain parts of chapters 2 and 3 have been taken from that project. Specifically, in Chapter 2, sections 2.2 and 2.3 have been partially reused. Similarly, in Chapter 3, the vessel modeling and certain derived contact forces have been extracted from the specialization project and incorporated into this thesis.

First and foremost, I would like to express my gratitude to my supervisor, Tor Arne Johansen (NTNU), and Øyvind Smogeli (NTNU/Zeabuz), for offering me the opportunity to work on this fascinating project. Additionally, I would like to extend my thanks to my co-supervisor, Emil Hjelseth Thyri (Zeabuz), for their valuable feedback and assistance whenever I needed it.

Jonas Anker Horntvedt

Trondheim, June 2023

Table of Contents

Summary i

Sammendrag iii

Preface v

Table of Contents ix

List of Tables xi

List of Figures xvii

1 Introduction 1

1.1 Background 1

1.2 Motivation 5

1.3 Problem description 6

1.4 Contributions 7

1.5 Outline 8

2 Theory 9

2.1 Literature Review 9

2.2 Dynamics of a marine craft 11
2.3 Guidance 13

3 Implementation **15**
3.1 The vessel 15
3.2 Modeling 16
3.2.1 Wind modeling 16
3.2.2 Otter Model 18
3.2.3 Contact forces between vessel and docking platform 20
3.2.4 Improvements of the contact forces 24

4 Operation phases **27**
4.1 Transit and docking routine 27
4.2 Control overview transit and docking 28
4.2.1 Transit state monitor 30
4.2.2 Course guidance 31
4.2.3 Speed guidance 32
4.2.4 Transit state controller 32
4.2.5 Course reference model 34
4.2.6 Velocity reference model 35
4.2.7 Course PID-controller 35
4.2.8 Surge PI-controller 36
4.3 Undocking routine 36
4.4 Control overview undocking 37
4.4.1 Undocking state monitor 37
4.4.2 Course guidance 38
4.4.3 Speed guidance 38
4.4.4 Undocking state controller 38

5 Simulation results **39**

5.1 Parameters 40

5.2 Route 41

5.3 Undocking results 43

5.4 Transit results 44

5.5 Docking results 44

5.5.1 Scenario 1 45

5.5.2 Scenario 2 51

5.5.3 Scenario 3 65

5.5.4 Scenario 4 69

5.6 Discussion 70

6 Conclusion and further work **71**

Bibliography **73**

List of Tables

2.1 Table for the 3DOF SNAME (1950) notation 13

5.1 Parameters used in the thesis 40

5.2 **Scenario 2:** A tabular representation indicating the wind speeds at which the maximum U_{impact} is attained for every direction of the wind. 53

5.3 **Scenario 2:** A tabular representation indicating the wind speeds at which the maximum p_{impact} is attained for every direction of the wind. 55

5.4 **Scenario 2:** A tabular representation indicating the wind speeds at which the maximum time to fully docked is attained for every direction of the wind. 59

5.5 **Scenario 2:** The ψ_{impact} in the interval for highest $T_{docking}$ for -135, 180 and 135°. 64

5.6 **Scenario 2:** A heatmap that shows the different surge metrics calculated for the different wind directions and speeds. The Wind direction is in degrees relative to the north. The heatmap is scaled between the maximum surge metric of 0.792, and the minimum surge metric of 0.130. 64

5.7 **Scenario 2:** A heatmap that shows the different course metrics calculated for the different wind directions and speeds. The Wind direction is degrees relative to the north. The heatmap is scaled between the maximum course metric of 1.499 and the minimum surge metric of 29.91. To minimize the span, all values have been divided by 10. 65

5.8 **Scenario 4:** The docking criteria for -135°for different turning points . . 69

List of Figures

1.1 Robots in use 2

1.2 The world's first electric and fully autonomous cargo ship Yara Birkeland. Courtesy of Tomas Østberg-Jacobsen (Optima, 2023). 3

1.3 The world's first autonomous passenger ferry milliAmpere 2 that did a trial in Trondheim. Courtesy of Kai T. Dragland. 3

1.4 The sequence of docking a boat using spring lines (BoatUS, 2013). 5

1.5 Paris river shuttle that operates in the channels of Paris. These shuttles are underactuated and electric. Courtesy of Øyvind Smogeli. 5

1.6 A docking hitch that is used to simplify docking for underactuated vessels. The passenger ferries in Paris are installed with such hitch as pictured here, and the Otter model used in this thesis is supplied with one as well. Courtesy of Øyvind Smogeli. 6

1.7 A docking receiver that is used to simplify docking for underactuated vessels. This receiver is installed in the docks in Paris to mate with docking hitches equipped on the ferries. The dock in the simulation environment will be modeled with such a docking receiver. Courtesy of Øyvind Smogeli. 7

2.1 The Piraya, an experimental USV platform developed by Saab Kockums (Saab, 2022). The vessel is underactuated with only an outboard engine at the back. Picture is from (Kockum, 2022). 11

2.2 An illustration of a 6-DOF surface vessel, illustrating surge, sway, heave, roll, pitch, and yaw with the body-fixed reference frame.(Fossen, 2021) . 12

2.3 How the LOS Guidance principle is used to calculate the course reference given by the vessel's position and two waypoints. Courtesy of (Fossen, 2021) 14

3.1 The USV Otter, an unmanned surface vessel platform developed by Maritime Robotics (Robotics, 2022). 16

3.2 Wind modeling parameters (Fossen, 2021). Including wind speed V_w, wind direction β_w, and the wind angle of attack γ_w. 17

3.3 The modeled docking adapter with the hitch as a circle and the receiver split up into $l1$, $l2$, and $l3$. The other side of the line that is connected to the circle is connected to the vessel. 20

3.4 The third polynomial function given by the values chosen by $\boldsymbol{\delta}$ and $\mathbf{F}_{\mathbf{contact}}$ as well as the plotted for $\boldsymbol{\delta}$ and $\mathbf{F}_{\mathbf{contact}}$ 21

3.5 Contact force tests 22

3.6 Contact force fx while the boat tries to stay still in the docking adapter, but is bumping in the docking receiever. 22

3.7 The vector between CO and CA. 23

3.8 Contact force fx while the boat stays still in docking adapter. 23

3.9 The contact geometry between the docking hitch illustrated by the circle, and $l2$, which is one of the lines that make up the docking receiver. Both angles are relative to the north. 24

4.1 The vessel arrives from transit into the docking area, approaches the turning point where it turns, and finally mates the hitch into the receiver (dashed grey) and rotates the vessel's aft into the pier. 28

4.2 Guidance, navigation, and control pipeline utilized in the simulations. The course and speed guidance vary for each state, and the yellow box accurately tracks the current state of the vessel and is illustrated in Figure 4.3. 29

4.3 Transit state monitor that determines whether the vessel should progress to the next state based on specific conditions within brackets [] assigned to each state and tracks what state the vessel is in. 30

4.4 The yaw rate during the docking rotation with a constant moment applied. The yaw rate increases even if the moment is constant because of the angle between the vessel and the wind changes. The wind speed is 7m/s, and the wind direction is parallel with the pier in this case. 33

4.5 The yaw rate of the vessel during the time between the hitch being connected to the receiver and when the vessel is fully docked when the wind speed is 7m/s, and the wind direction is parallel with the pier. A PID controller controls the yaw moment. 34

4.6 The undocking sequence begins with the vessel in a docked position (represented by dashed grey along the pier). Subsequently, the vessel rotates in the receiver until it achieves a certain angle in relation to the pier. Following this, it reverses to a safe distance from the pier (indicated by dashed grey at the turning point). The vessel then rotates towards the first transit point and ultimately proceeds to approach it. 36

4.7 The control overview which is quite similar to the one for transit and docking. The State monitor and state controller are different. 37

4.8 The state monitor used for tracking the undocking states. 37

5.1 The full route the vessel travels from $p_{starting}$ to $p_{docking}$ through $p_{turning}$. 41

5.2 The states during the full route. Remark that the plot starts after 140s, it is in transit for t $\in$ [0,157.1], the blue line. The second state is the Turning point approach, the orange line. The third state is the Turn state, the yellow line. The fourth state is the Approach Docking state, the purple line. The fifth state is Docking rotation and slide state, the green line. The final state is the Stay state which says the vessel is fully docked, the turquoise line. . 42

5.3 The propeller revolutions during the full route, from $p_{starting}$, to fully docked. Remark that the maximum rad/s is 103, and the minimum rad/s is -101 for The Otter. 42

5.4 The undocking operation for all wind direction and wind speed 7m/s. The vessel undocks at $p_{docking}$, turns toward the transit point when the distance to the pier is 2.5m, then travels to $wp_1 = [10, 20]$ 43

5.5 All vessel trajectories when experiencing 7m/s for each wind direction. The vessel travels from $p_{starting}$ to p_{ending}. 44

5.6 **Scenario 1:** U in the final seconds before and right after impact with the pier or receiver. 46

5.7 **Scenario 1:** The docking hitch's y position in NED during the final seconds of the docking, including the time of impact. 47

5.8 **Scenario 1:** ψ during the approach docking state, and T_{impact}. 47

5.9 **Scenario 1:** The time span where the docking hitch first hits the pier, blue line, and then slides into the receiver. Finally, the hitch is mated with the receiver, orange line, until the fully docked state is achieved, yellow line, as the vessel's side is in contact with the pier while the docking adapters are connected. The plot starts in the transition between the approach docking state and contact with the pier. 48

5.10 **Scenario 1:** The course metric during the approach docking state 49

5.11 **Scenario 1:** The course and desired course plot during the approaching docking state. 49

5.12 **Scenario 1:** The surge metric during the approach docking state 50

5.13 **Scenario 1:** The U and u_d plot during the approaching docking state. . . 51

5.14 **Scenario 2:** The maximum U_{impact} according to each wind direction. . . 52

5.15 **Scenario 2:** The maximum u_{impact} according to each wind direction. . . 52

5.16 **Scenario 2:** The average U_{impact} according to each wind direction 54

5.17 **Scenario 2:** The average u_{impact} according to each wind direction 54

5.18 **Scenario 2:** The maximum p_{impact} according to each wind direction . . . 55

5.19 **Scenario 2:** The average p_{impact} according to each wind direction 56

5.20 **Scenario 2:** The maximum α_{impact} according to each wind direction . . 57

5.21 **Scenario 2:** The average impact angle according to each wind direction . 58

5.22 **Scenario 2:** The maximum docking time according to each wind direction 59

5.23 **Scenario 2:** The average docking time according to each wind direction . 60

5.24 **Scenario 2:** The maximum docking according to each wind direction . . 60

5.25 **Scenario 2:** The minimum docking according to each wind direction . . . 61

5.26 **Scenario 3:** The three wind directions that have the biggest differences between maximum and minimum $T_{docking}$ for all wind speeds. 62

5.27 Impact points and impact angles for the three wind directions that have the biggest time differences between maximum and minimum docking times. 63

5.28 **Scenario 3:** The χ and χ_d plot during the approaching docking state with wind direction -135 degrees and 7m/s wind speed. 66

5.29 **Scenario 3:** The U, u, and u_d plot during the approaching docking state with wind direction -135 degrees and 7m/s wind speed. 67

5.30 The desired and actual yaw moment N during the approach docking state. 68

Chapter 1

Introduction

This chapter provides background information and motivation for the work done in this Master's thesis. The problem description is defined, as well as the contributions by the author to the project; finally, an outline of the report is given.

1.1 Background

Automation has significantly impacted the way humans perform tasks. Everyday chores, such as dishwashing and laundry, have been automated to save time and effort. The implementation of automation in the industry has also been instrumental in increasing efficiency and reducing costs. Removing humans from certain operations can decrease the risk of human accidents. In recent decades, robots have become increasingly prevalent in daily life, with robotic lawnmowers and vacuum cleaners now commonplace in households. Robots are also used in professional environments such as hospitals for tasks such as cleaning and carrying linen, meals, and medications (Robot, 2023), in warehouses (AutoStore, 2023), serving dining guests (Tech, 2023) and assembling electronic components (Reeco, 2023). Pictures of different robots that are in use are shown in Figure 1.1. The previously mentioned drones operate within controlled environments. However, implementing drones in more dynamic environments presents greater difficulties.

(a) An operative robot working in health care (GlobalData, 2023).

(b) Warehouse robots by AutoStore (AutoStore, 2023).

(c) BellaBot for serving dining guests. Courtesy of Aqilah Najwa Jamaluddin.

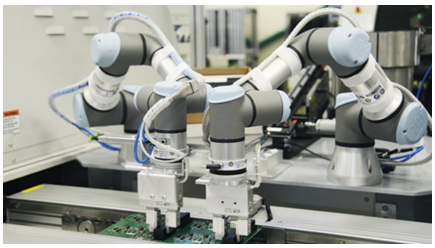

(d) Robot that assembles electronic components (Reeco, 2023).

Figure 1.1: Robots in use

Unmanned surface vessels (USVs) offer a wide range of uses, including the transportation of goods and people, seabed mapping, military applications, and gathering oceanographic and atmospheric data, among others (NOAA, 2023). USVs offer the additional advantage of cost reduction over time, as fewer crew members are required on board compared to boats operated by humans. This feature can potentially enhance the safety of the vessel's operation (Patterson et al., 2022). Seabed mapping and collecting oceanographic and atmospheric data are time-intensive tasks, making deploying autonomous USVs highly beneficial. These USVs can operate independently for extended periods, eliminating the need for human involvement. This approach proves to be cost-effective and has demonstrated promising outcomes (Centre, 2023). Furthermore, utilizing USVs for data collection presents the advantage of acquiring data in harsh environments without endangering human safety.

As waterways are often underutilized (Ceurstemont, 2023), USVs can be a viable alternative to reduce pressure on congested roads. In 2022, the inaugural journey of the world's first fully electric and entirely autonomous cargo ship pictured in Figure 1.2 was successfully accomplished (Technology, 2023). Once this vessel becomes operational, it is projected to reduce carbon dioxide emissions by 1,000 tonnes and replace approximately 40,000 diesel truck trips annually, highlighting electrical USVs' environmental benefits.

Figure 1.2: The world's first electric and fully autonomous cargo ship Yara Birkeland. Courtesy of Tomas Østberg-Jacobsen (Optima, 2023).

The versatility of USVs extends beyond transporting goods, as they are also capable of carrying humans. They can serve as replacements for conventional ferries and even open up new routes that would not be economically viable for human-operated boats. Autonomous passenger ferries can provide transportation for shorter distances, eliminating the need for costly bridge or tunnel constructions. In 2022, Trondheim it was conducted a successful trial of the world's first autonomous passenger ferry, The milliAmpere 2 (Haugan, 2023). During the trial, which lasted for several weeks, public members could board the ferry while researchers gathered feedback on their experiences (see Figure 1.3).

Figure 1.3: The world's first autonomous passenger ferry milliAmpere 2 that did a trial in Trondheim. Courtesy of Kai T. Dragland.

To achieve full autonomy in USVs, the entire operation must be automated. Typically, the operation is divided into three stages when a marine craft travels from one dock to another: undocking, transit, and docking. Undocking involves the boat moving safely away from the docking station, while transit refers to the transport stage where the vessel

follows a designated path or trajectory between the docking areas. The docking stage is the most complex and critical operation as it requires the boat to slow down and maneuver carefully to avoid collisions with the docking station or nearby objects such as piers. The slow speed hinders maneuverability, making the docking stage particularly challenging (Hendricks, 2012). This applies for underactuated vessels; for fully actuated vessels, the system works better at low speeds.

Docking is already a complex task and becomes even more challenging when dealing with underactuated vessels. The milliAmpere 2, however, is a fully actuated vessel, meaning it possesses the same number of actuators, or more, as degrees of freedom (DOF). Typically, there are 6 DOF, encompassing position and orientation represented by x, y, and z coordinates, as well as rotation around each axis. However, surface vessels often simplify this to 3 DOF. In the case of 3 DOF, the position is described by the coordinates $[x, y]$, while the vessel's orientation is determined by its heading, which is the rotation around the z-axis.

Underactuated USVs typically possess the capability to apply force in the x-direction and control the moment around the z-axis while lacking the ability to generate force in the y-direction. Achieving such underactuated capabilities in USVs can be accomplished through various combinations of actuators, such as a propeller and a rudder positioned at the aft, fixed propellers located at the aft, azimuth propellers installed at the aft, and other configurations. If the underactuated vessel has the rudder/propeller setup, the vessel needs speed to have yaw-actuation.

Due to the limited ability of vessels to exert forces in every direction, the docking process becomes particularly difficult when faced with environmental disturbances. When a crosswind or current occurs, the vessel experiences a sideward force that can push it off its intended course. Since there are no direct means to counteract these disturbances, the vessel must rely on a combination of lateral force and rotational moment (x force and z moment) to regain the correct course.

Various systems, such as docking adapters and spring lines, are available to assist underactuated vessels during the docking process. Captains have long relied on spring lines to facilitate docking, especially in unfavorable weather conditions. A spring line is fastened from the bow to the dock. The vessel's bow can be maneuvered towards the pier by thrust and the tension in the line. Once the bow is in position, the spring line aids in maintaining the boat's position while the rudder and propeller are employed to rotate the vessel's aft towards the pier, aligning it parallel to the docking area (BoatUS, 2013), the sequence is illustrated in Figure 1.4

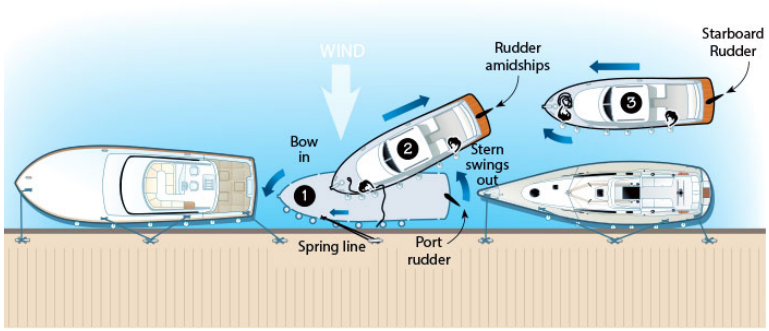

Figure 1.4: The sequence of docking a boat using spring lines (BoatUS, 2013).

1.2 Motivation

This thesis is motivated by developing automated docking for underactuated vessels to be used in underactuated autonomous operations. Underactuated USVs may be used due to cost-effectiveness, fewer actuators, or the incorporation of older boats with autonomy. The underactuated vessels that motivate this thesis cannot direct force sideways and, therefore, must follow a predefined trajectory that matches their actuator setup. An example of an underactuated vessel is the autonomous Paris river shuttle which is pictured in Figure 1.5. This thesis will focus on underactuated marine crafts, with a specific emphasis on developing a secure and robust docking scheme and their transit and undocking operations.

Figure 1.5: Paris river shuttle that operates in the channels of Paris. These shuttles are underactuated and electric. Courtesy of Øyvind Smogeli.

1.3 Problem description

This Master's thesis concerns the issue of docking underactuated vessels. The undocking and transit processes will also be addressed to provide a complete dock-to-dock solution. However, the primary focus of the thesis will be on the docking operation. A simulation environment will be utilized to test the undocking, transit, and docking operation. The simulation will employ an underactuated vessel modeled after Maritime Robotics' The Otter (Robotics, 2022) but is modeled with a docking hitch as shown in Figure 1.6.

Figure 1.6: A docking hitch that is used to simplify docking for underactuated vessels. The passenger ferries in Paris are installed with such hitch as pictured here, and the Otter model used in this thesis is supplied with one as well. Courtesy of Øyvind Smogeli.

The docking hitch cannot operate independently; it requires a receiver to connect with. As a result, a docking receiver needs to be modeled at the docking point in the simulation environment, as shown in Figure 1.7. The objective of the docking operation will be to safely connect the docking hitch with the receiver and adequately align the vessel with the pier.

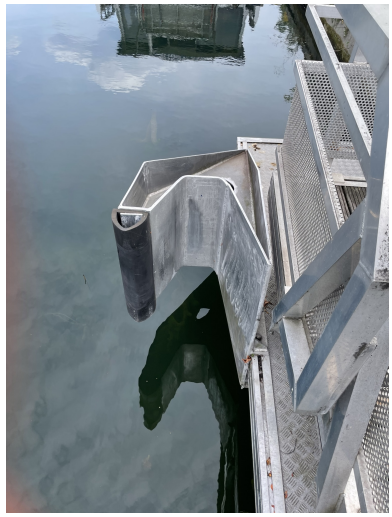

Figure 1.7: A docking receiver that is used to simplify docking for underactuated vessels. This receiver is installed in the docks in Paris to mate with docking hitches equipped on the ferries. The dock in the simulation environment will be modeled with such a docking receiver. Courtesy of Øyvind Smogeli.

The objectives of this thesis are:

- To develop a simulation environment for testing the underactuated vessel
- Develop a full dock-to-dock scheme regarding undocking, transit, and docking.
- Verify the performance of the operation under varying wind conditions through simulations.

1.4 Contributions

The main contributions of the work presented in this Master's thesis are as follows:

- A comprehensive simulation environment developed in Matlab and Simulink to assess undocking, transit, and docking. The simulation features a model of The Otter, complete with a docking hitch. In addition, a docking station equipped with a pier and docking receiver has been included in the environment. The contact forces between the vessel and docking station have been computed and integrated into the simulation. To determine how well the vessel performs under windy conditions, wind modeling has been incorporated into the simulation environment.

- Guidance and control mechanisms for undocking, transit, and docking. The undocking process has been separated and is not directly connected to the transit phase but rather prepares the vessel for transit. The transit and docking phases have been merged so the vessel can move through a series of waypoints, culminating in the docking area where it eventually docks.
- Evaluation of the operation solution within the simulation environment to determine the efficacy of the vessel's performance for different wind conditions.

1.5 Outline

The remainder of this thesis is structured as follows: Chapter 2 provides an overview of previous research on the topic and background theory. Chapter 3 describes the implementation of the various aspects of the simulation environment. Chapter 4 explains the different operational phases and how navigation and guidance were developed for each. In Chapter 5, the developed solution is tested within the simulation environment, and the results are analyzed. Finally, Chapter 6 concludes the report and offers suggestions for future work.

Chapter 2

Theory

This chapter provides a literature review, where previous work on the topic of automated docking is presented. The background theory used in the thesis is also provided.

2.1 Literature Review

The study by Walmsness et al. (2023) focuses on designing an automatic dock-to-dock control system for a passenger ferry that utilizes a bumpless transfer method. The paper breaks down the dock-to-dock process into three distinct phases: undocking, transit, and docking. The undocking phase is when the vessel leaves the dock. The transit phase is when the vessel navigates through open waters to reach its destination. Finally, the docking phase is when the vessel arrives at a specific location in the harbor to dock. The different phases have independent control strategies, and the paper suggests a solution where the vessel can switch between the control strategies without discontinuous jumps in the control action and lingering integral effects. The bumpless transfer solution uses the integral action of the receiving controller. This is done by enforcing the two controllers to be equal during the transition and solving the integrator state value. The solution was tested in a simulator. The results show that the bumpless transfer solution successfully combines independent control regimes, taking the ferry from one dock to another. Especially when transitioning from higher speed in transit to lower speed in docking is improved by using the proposed bumpless transfer solution. The docking controller used in the thesis is a DP controller, which requires a fully actuated vessel, and can, therefore, not be used for the underactuated vessels considered in this thesis. However, the concept of bumpless transfer is just as relevant for underactuated vessels.

Several solution proposals have been explored regarding automatic docking for underactuated surface vessels. Han et al. (2021) proposes an Extended Dynamic Window Approach

to perform the motion planning of automatic berthing. The approach takes all the dynamic constraints of the USV into account and obtains predicted trajectories the underactuated USV manages to follow. In real-time, the predicted trajectories are compared to static and, if known, dynamic obstacles. The trajectories that collide with the obstacle get discarded. The remaining trajectories are evaluated by an objective function to select the optimal trajectory. The results are obtained from simulations using CyberShip II (Skjetne et al., 2004). The results show that the USV successfully docks at different desired positions and with different wind speeds and directions. The USV also manages to avoid the obstacles in the test. The test exclusively considers wind for external disturbances; waves and ocean currents are not accounted for. The effectiveness and robustness are not investigated in the paper. There are no infield experiments to validate the approach.

The docking of an underactuated USV using deep reinforcement learning (DRL) is explored in a study by Strand (2020). The author explores two DRL algorithms: deep deterministic policy gradient (DDPG) and proximal policy optimization (PPO). Three cases are simulated to evaluate the DRL solution. The first case investigates the ability of both DRL algorithms to dock in the absence of ocean currents and measurement noise, with the results showing that PPO outperforms DDPG, although the thruster inputs from PPO are rapidly oscillating and are not realistic behavior. The second case examines the performance of only PPO with measurement noise but no ocean currents. The results show that the PPO algorithm performs well in such ideal conditions. In this case, the thruster input is smoother and might be explained by removing the penalty for not keeping the desired surge velocity. In the third case, the PPO algorithm is tested with measurement noise and ocean currents, and two scenarios are explored: one with known ocean currents and one with unknown ocean currents. The one with measured ocean current performed strictly better and was able to dock with ocean currents up to 4 m/s. The results suggest that further improvements are necessary, as only ocean currents were considered, other disturbances such as wind and waves were not, thruster dynamics were not considered, and the boat was allowed to dock up to 1 meter away from the desired docking point. In this thesis, a solution where the boat aims to lock a certain position and, therefore, motivates to find another docking solution.

The docking of underactuated surface vessels has been investigated using Model Predictive Control (MPC), as documented in a study by Kockum (2022), the vessel is pictured in Figure 2.1. The study uses simulations and physical tests to examine three distinct methods for advancing toward a desired position. In addition, obstacle avoidance is implemented. The MPC controller is utilized in three different approaches to docking. The first approach involves one target position, where the MPC controller is given a single target position and determines the optimal path on its own. The second approach involves following different waypoints into docking, while the final approach involves following a pre-recorded trajectory created by the vessel. Both simulated and experimental results are favorable as they approach the desired endpoint with the correct heading. However, it is worth noting that the endpoint is a waypoint in open waters, and thus it is unclear how the offset results would affect the vessel when docking at a pier. Additionally, the vessel used in this study has only been tested under moderate winds, not strong ones.

Figure 2.1: The Piraya, an experimental USV platform developed by Saab Kockums (Saab, 2022). The vessel is underactuated with only an outboard engine at the back. Picture is from (Kockum, 2022).

The mentioned docking methods have demonstrated favorable outcomes under specific circumstances. Nevertheless, neither incorporates the unique docking adapter in the USV considered in this thesis. This discrepancy serves as a motivation to explore a docking solution that leverages the advantages offered by the docking adapter.

2.2 Dynamics of a marine craft

The theory utilized in this thesis is identical to that of Horntvedt (2022) and has been obtained from the aforementioned thesis.

The dynamics of a marine craft are divided into two parts in Fossen (2021); kinematics and kinetics. Kinematics is the position and orientation without considering the forces/torques that cause the motion (Waldron et al., 2016). On the other hand, kinetics considers how the forces are causing the motions. A marine craft has 6 degrees of freedom (DOF). The 6 DOFs are motions and rotations about x, y, and z; see Figure 2.2.

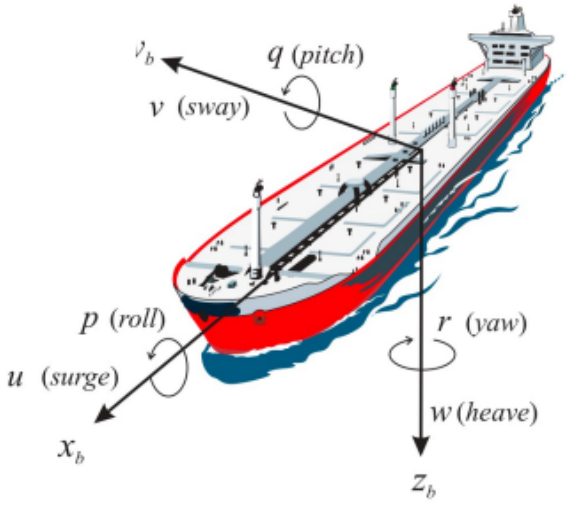

Figure 2.2: An illustration of a 6-DOF surface vessel, illustrating surge, sway, heave, roll, pitch, and yaw with the body-fixed reference frame.(Fossen, 2021)

Regarding control, Unmanned aerial vehicles (UAVs) and Autonomous Underwater Vehicles (AUVs) utilize all 6DOF, while for USVs, typically only 3DOF - surge, sway, and yaw are considered. Therefore, the remainder of this thesis focuses on the 3 DOF relevant to USVs.

Different reference frames are used to describe the position and orientation of a marine craft. In this thesis, body-fixed frame BODY and North-East-Down frame NED are used. The notation for The BODY frame and NED frame are often $\{\mathrm{b}\}$ and $\{\mathrm{n}\}$.

The NED frame is a geographic reference frame denoted $\mathrm{n} = (x_n, y_n, z_n)$ where x_n is pointing towards true North, y_n is pointing towards East, and z_n is pointing downwards. The origin o_n is chosen and is defined relative to Earth's reference ellipsoid. NED is used commonly used for local navigation (Fossen, 2021).

The BODY is a body-fixed reference frame denoted $\mathrm{b} = (x_b, y_b, z_b)$. The reference frame moves along with the craft and is often defined with o_b in the geometric center of the craft coinciding with the waterline. x_b is directed from aft to fore, y_b is pointing towards starboard and z_b is directed from top to bottom.

The 6DOF linear and rotational motions in BODY are illustrated in Figure 2.2. For 3DOF, the position is described by x and y, while the translation motion is defined by the linear velocities u and w. The Euler Angles represent the orientation, and ψ and its corresponding rotational velocity r are considered. The position is often described as the NED position, while the orientation is The Euler Angles between BODY and NED. This notation is the SNAME notation and is presented in SNAME (1950).

DOF	Forces and moments	Linear and angular velocities	Positions and Euler Angles
Motions in the x_b-direction(surge)	X	u	x^n
Motions in the y_b-direction(sway)	Y	v	y^n
Rotation about the z_b-axis(yaw)	N	r	ψ

Table 2.1: Table for the 3DOF SNAME (1950) notation

The equations of motion are given in the following matrix-vector form (Fossen, 2021):

$$\dot{\boldsymbol{\eta}} = \boldsymbol{J}_{\boldsymbol{\Theta}}(\boldsymbol{\eta})\boldsymbol{\nu}, \tag{2.1}$$

$$\mathbf{M}\dot{\boldsymbol{\nu}} + \mathbf{C}\boldsymbol{\nu} + \mathbf{D}(\boldsymbol{\nu})\boldsymbol{\nu} + \mathbf{g}(\boldsymbol{\eta}) + \mathbf{g}_0 = \boldsymbol{\tau} + \boldsymbol{\tau}_{wind} + \boldsymbol{\tau}_{wave}, \tag{2.2}$$

where $\mathbf{M}$ is the inertia matrix, $\mathbf{C}$ is the coriolis matrix, $\mathbf{D}$ is the damping matrix, $\mathbf{g}(\boldsymbol{\eta})$ is the generalized gravitational and buoyancy force-matrix, and $\mathbf{g}_0$ consists of static restoring forces and moments due to ballast systems and water tanks. $\boldsymbol{\tau}$ represents the forces for the actuators on the vessel, $\boldsymbol{\tau}_{wind}$ represents the forces performed by the wind on the vessel, and $\boldsymbol{\tau}_{wave}$ is the forces of the waves performed on the vessel. The matrices $\boldsymbol{\eta}$ and $\boldsymbol{\nu}$ are

$$\boldsymbol{\eta} = \begin{bmatrix} x^n, & y^n, & \psi \end{bmatrix}^T, \tag{2.3}$$

$$\boldsymbol{\nu} = \begin{bmatrix} u, & v, & r \end{bmatrix}^T, \tag{2.4}$$

The vessel model applied in this project will be defined later in the thesis.

2.3 Guidance

Guidance is "The process for guiding the path of an object towards a given point, which in general may be moving" Shneydor (1998). A popular guidance method for maritime surface vessels is line-of-sight (LOS) guidance. LOS will ensure that the vessel tracks a path by a set of predefined waypoints and decide the course reference based on the cross-track error to the line between the waypoints. LOS will not direct the vessel to the closest point on the path but rather a user-specified lookahead distance down the path. The distance to the path and the lookahead distance affects how the vessel approaches the path. The LOS principle is illustrated in Figure 2.3. The proportional LOS Guidance law is (Fossen, 2021):

$$\chi_d = \pi_p - \arctan(\mathrm{K_p} y_e^p), \tag{2.5}$$

$$\pi_p = \text{atan2}(\text{y}_{i+1}^n - y_i^n, x_{i+1}^n - x_i^n), \tag{2.6}$$

$$y_e^p = -(x^n - x_i^n)\text{sin}(\pi_p) + (y^n - y_i^n)\text{cos}(\pi_p). \tag{2.7}$$

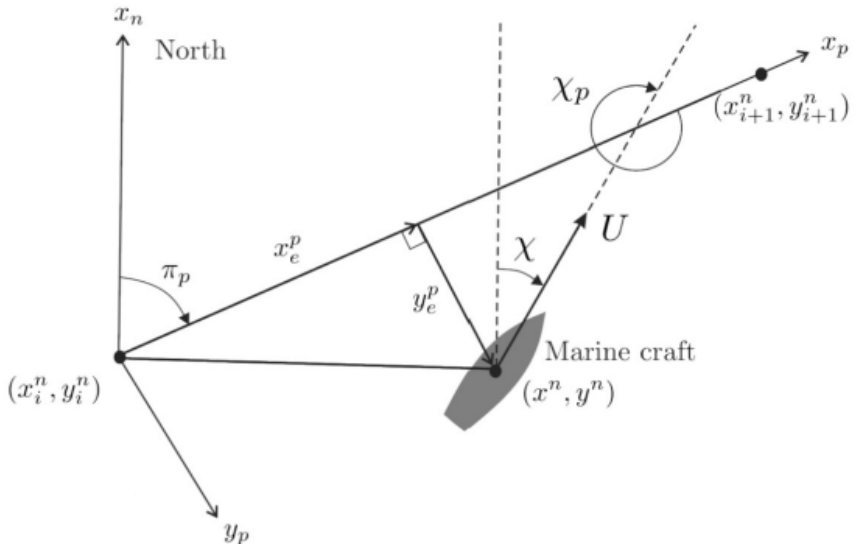

Figure 2.3: How the LOS Guidance principle is used to calculate the course reference given by the vessel's position and two waypoints. Courtesy of (Fossen, 2021)

$K_p = \frac{1}{\Delta}$ where Δ is the user-specified lookahead distance. The desired course χ_d is given by (2.5), the relationship between heading ψ and χ is

$$\chi = \psi + \beta_c. \tag{2.8}$$

The heading is the direction the vessel is pointing, while the course is the direction the vessel is moving. GNSS can measure course, but the vessel needs a noticeable positive speed. One way to determine the course is by using the relationship in Equation (2.8) if the crab angle β_c is known. However, the course may be unreliable when the value of u is close to zero, as the calculation of the crab angle, is

$$\beta_c = \text{arctan}(\frac{v}{u}). \tag{2.9}$$

In this case, the course may be subject to large errors or become undefined.

Chapter 3

Implementation

To accurately simulate the docking sequence, a simulator must be developed. The present thesis employs Matlab and Simulink to create an environment that mirrors the conditions typically encountered by marine vessels. Specifically, the focus is on river shuttles that navigate through calm channels with negligible currents or waves but may face windy conditions. The simulator environment is designed to incorporate wind but not current or waves. To capture the behavior of the passenger ferries, the simulator employs an underactuated Otter model, modeled with a docking hitch to simplify the docking routine. The interaction between the hitch and receiver is included in the simulation to provide a more comprehensive analysis of the dock-to-dock process.

3.1 The vessel

Within the simulation environment, the vessel is simulated using a model of the USV Otter developed by Marine Robotics. This model incorporates two fixed electric thrusters positioned at the rear of the vessel. Since the thrusters are fixed, the rotation around the z-axis is accomplished by adjusting the speeds of each thruster independently. The Otter, being a small USV, does not have the capacity to transport passengers. However, it serves as an effective platform for experimenting with and evaluating the principles of underactuated vessels.

Figure 3.1: The USV Otter, an unmanned surface vessel platform developed by Maritime Robotics (Robotics, 2022).

3.2 Modeling

This section presents the modeling of all components included in the simulation environment. Initially, the wind's external disturbance is modeled, followed by the modeling of the USV The Otter. Lastly, the derivation of the contact forces' modeling is provided.

3.2.1 Wind modeling

Ocean currents and waves are minimal in waterways, yet wind remains a factor. The simulator will consider the wind to get as good results as possible. Wind for a symmetrical ship in motion can be modeled as in Fossen (2021)

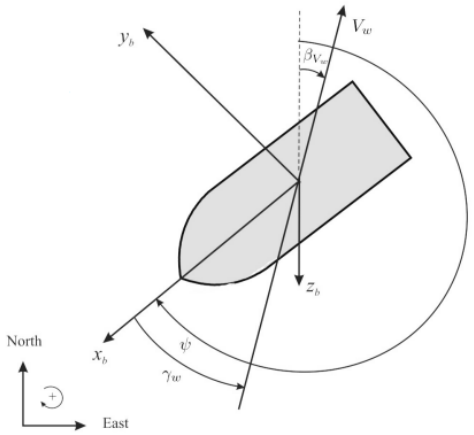

Figure 3.2: Wind modeling parameters (Fossen, 2021). Including wind speed V_w, wind direction β_w, and the wind angle of attack γ_w.

$$\tau_{wind} = \frac{1}{2}\rho_a V_{rw}^2 \begin{bmatrix} C_X(\gamma_{rw})A_{F_w} \\ C_Y(\gamma_{rw})A_{L_w} \\ C_N(2\gamma_{rw})A_{L_w}L_{oa} \end{bmatrix}, \tag{3.1}$$

where ρ_a is the air density, V_{rw}^2 is the relative wind speed, γ_{rw} is the wind angle of attack, A_{F_w} and A_{L_w} are the frontal and lateral areas and L_{oa} is the overall length of the vessel. The wind coefficients C_X, C_Y and C_N can be calculated according to Blendermann (1994). To calculate V_{rw} the relative velocities u_{rw} and v_{rw} have to be used. The relative velocities are calculated using the x and y components of V_w from Figure 3.2.

$$u_w = V_w \cos(\beta_{V_w} - \psi), \tag{3.2a}$$
$$u_w = V_w \sin(\beta_{V_w} - \psi), \tag{3.2b}$$

then the relative velocities are

$$u_{rw} = u - u_w, \tag{3.3a}$$
$$u_{rw} = v - v_w, \tag{3.3b}$$

the relative wind speed is

$$V_{rw} = \sqrt{u_{rw}^2 + v_{rw}^2}, \tag{3.4}$$

and the relative angle of attack is

$$\gamma_{rw} = -\text{atan2}(v_{rw}, u_{rw}). \tag{3.5}$$

3.2.2 Otter Model

The Otter model used in the simulations is already derived in Horntvedt (2022), and this part is obtained from that.

Kinematics

The matrices for kinematics are derived in 6 DOF in another Master's thesis (Strand, 2020). This thesis will use the same matrices for the Otter but focus on the 3 DOF; surge, sway, and yaw. All the matrices are derived in the control origin CO. The first matrix is the inertia matrix for the ship in CO $\mathbf{M}_{RB}^{CO}$;

$$\mathbf{M}_{RB}^{CO} = \begin{bmatrix} m+mp & 0 & -y_g(m+mp) \\ 0 & m+mp & x_g(m+mp) \\ -y_g(m+mp) & x_g(m+mp) & m*R_{66}^2 + x_g^2(m+mp) + y_g^2(m+mp) \end{bmatrix}, \tag{3.6}$$

where m is the boat's mass, mp is the mass of the payload, x_g and y_g is the distance from the center of gravity to the control origin in x and y direction in the body frame, R_{66} is the radii of gyration about the z axis. The second matrix is the rigid-body coriolis and centripetal forces-matrix

$$\mathbf{C}_{RB}^{CO}(\boldsymbol{\nu}) = \begin{bmatrix} 0 & -r(m+mp) & -rx_g(m+mp) \\ r(m+mp) & 0 & -ry_g(m+mp) \\ rx_g(m+mp) & ry_g(m+mp) & 0 \end{bmatrix}, \tag{3.7}$$

where r is the yaw rate. $\mathbf{M}_{RB}^{CO}$ and $\mathbf{C}_{RB}^{CO}(\boldsymbol{\nu})$ are the rigid-body kinematics, the resistance of the fluid has to be accounted for as well. This is done by including hydrodynamic added mass $\mathbf{M}_A$ and $\mathbf{C}_A(\boldsymbol{\nu})$;

$$\mathbf{M}_A = -\begin{bmatrix} X_{\dot{u}} & 0 & 0 \\ 0 & Y_{\dot{v}} & 0 \\ 0 & 0 & N_{\dot{r}} \end{bmatrix}, \tag{3.8}$$

$$\mathbf{C}_A(\boldsymbol{\nu}) = \begin{bmatrix} 0 & 0 & Y_{\dot{v}}v \\ 0 & 0 & -X_{\dot{u}}u \\ -Y_{\dot{v}}v & X_{\dot{u}}u & 0 \end{bmatrix}, \tag{3.9}$$

These assumptions were made according to Strand (2020);

$$X_{\dot{u}} = -0.1 \cdot m \tag{3.10a}$$
$$Y_{\dot{v}} = -1.5 \cdot m \tag{3.10b}$$
$$N_{\dot{r}} = -1.7 \cdot R_{66} \tag{3.10c}$$

Restoring forces

By the assumptions that roll and pitch are small, the following matrix $\mathbf{g}(\boldsymbol{\eta})$ is :

$$\mathbf{g}(\boldsymbol{\eta}) = \begin{bmatrix} 0 \\ 0 \\ 0 \end{bmatrix}, \tag{3.11}$$

With the assumption $\mathbf{g}(\boldsymbol{\eta}) \approx \mathbf{G}\boldsymbol{\eta}$ (Fossen, 2021) $\mathbf{G}$ is also zeros in surge, sway, and yaw, the same yields for $\mathbf{g}_0$.

Damping Forces

The linear viscous damping matrix $\mathbf{D}(\boldsymbol{\nu})$ is:

$$\mathbf{D}(\boldsymbol{\nu}) = \begin{bmatrix} X_u & 0 & 0 \\ 0 & Y_v & 0 \\ 0 & 0 & N_r \end{bmatrix}, \tag{3.12}$$

Where (Strand, 2020)

$$-X_u = \frac{M_{11}}{T_{surge}} \tag{3.13a}$$
$$-Y_v = 0 \tag{3.13b}$$
$$-N_r = \frac{M_{66}}{T_{yaw}} \tag{3.13c}$$

The nonlinear damping is zero for surge, but the nonlinear damping in sway and yaw is given by Fossen (2021):

$$Y = -\frac{1}{2}\rho \int_{-\frac{L}{2}}^{\frac{L}{2}} T(x) C_d^{2D}(x) |v_r + xr|(v_r + xr) dx, \tag{3.14a}$$

$$N = -\frac{1}{2}\rho \int_{-\frac{L}{2}}^{\frac{L}{2}} T(x) C_d^{2D}(x) x |v_r + xr|(v_r + xr) dx, \tag{3.14b}$$

The values for Y and N are calculated with the function CrossFlowDrag in Matlab MSS toolbox (Fossen, 2022).

3.2.3 Contact forces between vessel and docking platform

In the simulation, the forces between the docking adapters and the contact forces between the vessel and the pier must be included. The base for this calculation is obtained from Horntvedt (2022).

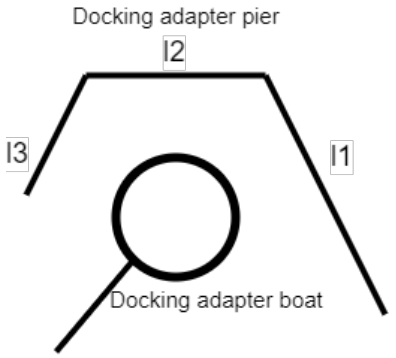

Figure 3.3: The modeled docking adapter with the hitch as a circle and the receiver split up into $l1$, $l2$, and $l3$. The other side of the line that is connected to the circle is connected to the vessel.

Contact force magnitude

The docking receiver is modeled as three straight line segments, denoted $l1$, $l2$, and $l3$. The receiver and these three lines are illustrated in Figure 3.3. The docking hitch is considered elastic to model the contact force's magnitude F_{li}, where i represents which of the three contact surfaces that perform the force. The contact force is a function of how much the hitch is squeezed, which is the radius of the hitch r_{hitch} subtracted by how close the center is to the contact surface. The squeezing is defined as δ

$$\delta = |r_{hitch} - |d_{ai}||, \tag{3.15}$$

where $|d_{ai}|$ is the distance between the hitch and contact surfaces $l1$, $l2$ and $l3$. $r_{hitch} = 0.1$.

The relationship between δ and the magnitude of $\mathbf{F_{contact}}$ is modeled by using fitting a third-order polynomial. This is done using the "polyfit" (Mathworks, 2022). The fitting function uses x and y inputs and calculates coefficients for a third-order polynomial. The x-values indicate how much the circle is squeezed δ, and y decides how many Newtons the contact forces should perform. The x parameter is $\boldsymbol{\delta}$ in meters, and y parameter is $\mathbf{F_{contact}}$ in newtons. The values are chosen by reasonable estimates and is:

$$\delta = [0, 0.02, 0.06, 0.07], \tag{3.16}$$

$$\mathbf{F_{contact}} = [0, 60, 200, 700]. \tag{3.17}$$

The function $F_{contact}(\delta)$ is illustrated in Figure 3.4.

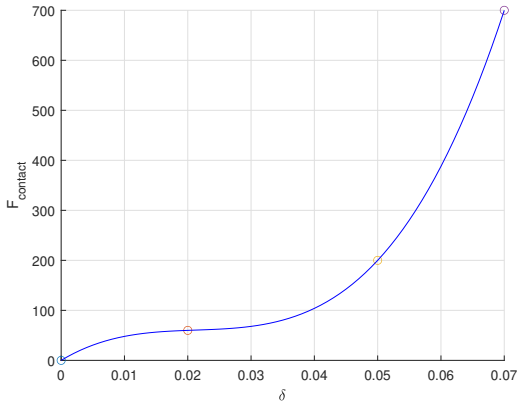

Figure 3.4: The third polynomial function given by the values chosen by $\boldsymbol{\delta}$ and $\mathbf{F_{contact}}$ as well as the plotted for $\boldsymbol{\delta}$ and $\mathbf{F_{contact}}$

Then the contact force magnitude is

$$F_{li}(\delta) = F_{contact}(\delta). \tag{3.18}$$

The values in (3.16) and (3.17) are not calculated; they are educated guesses. Since no physical system is available for calibration, the magnitude is based on empirical testing in the simulator. When the contact force, denoted as $\mathbf{F_{contact}}$, resembled the graph shown in Figure 3.4, the vessel experienced a higher velocity upon bumping back from the docking receiver compared to its initial arrival velocity. The equation underwent further adjustments through tuning efforts. This gave

$$F_{li}(\delta) = 0.1F_{contact}(\delta). \tag{3.19}$$

.

This brought the vessel to a stop without causing significant backward movement. The contact forces forced by the docking adapter before and after tuning are shown in Figure 3.5.

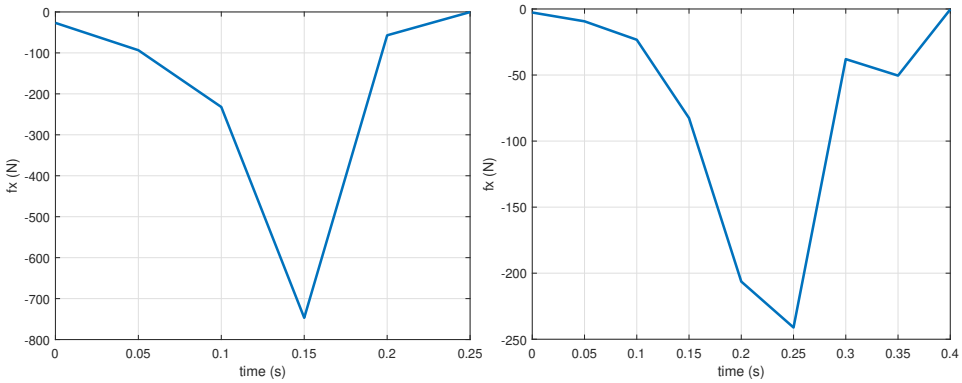

(a) Contact force fx during the first test, showing and undesirable outcome of almost -800N.

(b) Contact force fx achieved after tuning, which gave approximately -250N.

Figure 3.5: Contact force tests

The developed contact forces were tested in the simulation to ensure their accuracy and validity. The sequence was to drive straight to the docking adapter. The boat should be able to lie still in the docking adapter. However, as shown in Figure 3.6, there is some bumping between the docking adapters. Changing the values in (3.16) and (3.17) was tried to fix the bumping, but this did not solve the bumping part.

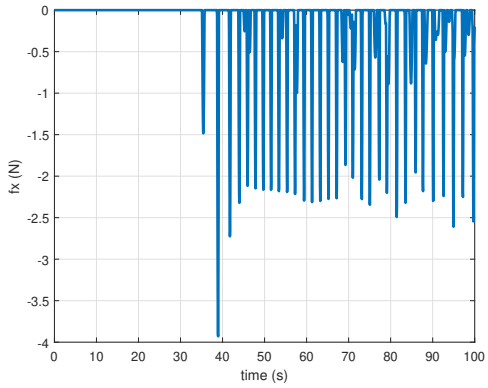

Figure 3.6: Contact force fx while the boat tries to stay still in the docking adapter, but is bumping in the docking receiever.

To solve the bumping, damping is included. The docking adapter will work more like a spring-damper system by including damping. When the boat's docking hitch moves towards the pier's docking receiver, the force will be greater than when the boat's hitch moves away. The docking hitch's linear velocities can be computed (Fossen, 2021)

$$\vec{v}_{na} = \vec{v}_{nb} + \vec{\omega}_{nb} \times \vec{r}_{ba}, \tag{3.20}$$

where $\vec{r}_{ba}$ is the vector between the control origin and the docking hitch as illustrated in 3.7, $\vec{\omega}_{nb}$ is the rotational velocity about BODY and $\vec{v}_{nb}$ is the linear velocity in BODY.

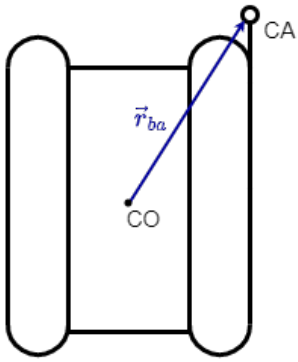

Figure 3.7: The vector between CO and CA.

To see if the $\vec{v}_{na}$ is moving towards or away from the contact surface, the dot product between $\vec{v}_{na}$ and the normal vector of the contact surface has to be analyzed. If the dot product is positive, the docking adapter moves away from the contact surface. The bumping was removed by reducing the force‘s magnitude for the positive dot product; conditional equations are

$$F_{li}(\delta) = \begin{cases} 0.1F_{contact}(\delta), & \text{if } \vec{v}_{na} \cdot \vec{n}_i \leq 0 \\ 0.001F_{contact}(\delta), & \text{otherwise} \end{cases} \tag{3.21}$$

where $\vec{n}_i$ is the normal vector for the corresponding contact surface.

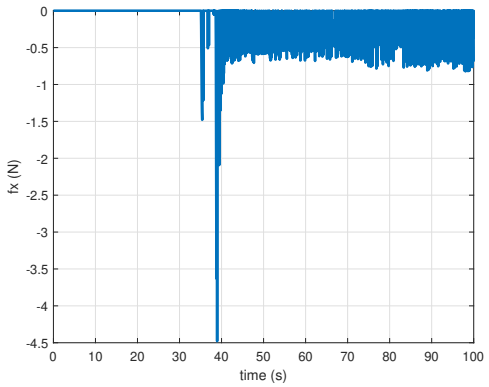

Figure 3.8: Contact force fx while the boat stays still in docking adapter.

Contact force angles

The angle between the receiver and the docking hitch must be calculated when calculating the contact forces. The angle between the hitch and the receiver is found from ψ, and the orientation of the dock, which is assumed to be known and constant. Both ψ and the orientation of the dock are relative to the north. The calculation derived in this section will be based on the angle between $l2$ and ψ, but it is done similarly with $l1$ and $l3$. An illustration of the angles is shown in Figure 3.9.

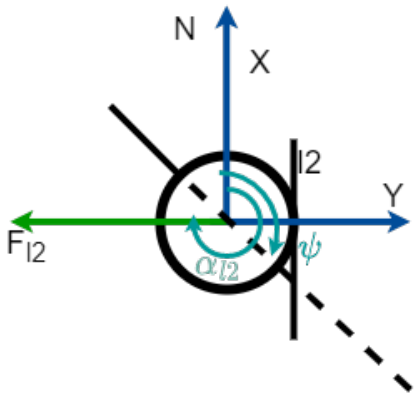

Figure 3.9: The contact geometry between the docking hitch illustrated by the circle, and $l2$, which is one of the lines that make up the docking receiver. Both angles are relative to the north.

α_{l2} is the angle between $l2$ and the north. The angle between α_{l2} and ψ is now defined as

$$\alpha_{cf} = \alpha_{l2} - \psi. \tag{3.22}$$

To decompose F_{li} into the boat's body frame, α_{cf} can be used. The force F_{l2} is decomposed in F_{l2x} and F_{l2y}, which is the force decomposed in the x and y in $\{\text{b}\}$

$$F_{l2x} = F_{l2} * cos(\alpha_{cf}), \tag{3.23}$$

$$F_{l2y} = -F_{l2} * sin(\alpha_{cf}). \tag{3.24}$$

3.2.4 Improvements of the contact forces

The subsections 3.2.2 through 3.2.3 were obtained from Horntvedt (2022). However, certain enhancements have been incorporated to achieve even more realistic simulations.

Fenders mounted on boat

In this thesis, the docking hitch is modeled to slide along the pier and into the docking receiver. In Horntvedt (2022), the fenders were mounted at the pier, which would hinder the sliding operation. Consequently, the fenders must be relocated from the pier to the boat. The fenders are mounted on the starboard side with distances of 0.6, 1.1, and 1.6 meters from the docking hitch. The position of fender i in NED is

$$\mathbf{p}_{fi}^n = \mathbf{p}_a^n - \mathbf{R}_n^b(\psi) \begin{bmatrix} d_{fia} & 0 & 0 \end{bmatrix}^{\mathrm{T}}, \tag{3.25}$$

where d_{fia} is the distance between fender i and the docking hitch and $\mathbf{p}_a^n$ is the position of the docking hitch. The distance between the pier and each fender is

$$d_{fip} = \frac{\parallel \overrightarrow{PF}_{fi} \times \overrightarrow{P} \parallel}{\parallel \overrightarrow{P} \parallel}, \tag{3.26}$$

where $\overrightarrow{PF}_{fi}$ is the vector between fender i and the pier, and $\overrightarrow{P}$ is the pier's vector. The contact force magnitude and angles are equally computed as previously in the section. The damping is equal to (3.21).

Contact between the pier and docking hitch

The docking hitch can now slide along the pier, which is implemented in the simulation. This is done in the exact way as in Section 3.2.3.

Chapter 4

Operation phases

This chapter will present a comprehensive overview of the entire dock-to-dock routine. The initial section will focus on describing the transit and docking procedures. In a previous study Horntvedt (2022), the same Unmanned Surface Vehicle (USV) with a docking adapter was examined. While achieving favorable outcomes through a curved path approach towards the docking receiver, it was observed that this method was susceptible to disturbance. As a result, an alternative docking approach is employed in this thesis.

Following the explanation of the routines, the control overview for both the transit and docking procedures is provided. Each aspect of the control overview is then elaborated upon in detail. Subsequently, the undocking routine is outlined along with its corresponding control overview. Finally, the new elements introduced in the control overview are elucidated.

4.1 Transit and docking routine

This thesis will explore the transit and docking routine, starting with the vessel in transit and following waypoints into the docking area where the docking sequence begins. Traditional guidance methods will be used during transit since these don't require fully actuated vessels, since the guidance only needs forward thrust as well as yaw moment. However, during docking, the underactuated vessel may face more severe limitations, particularly when under the influence of disturbances. In such cases, applying force in the y may be necessary, but with no actuator available to move the vessel sideways, the docking approach must therefore be carefully planned.

In Horntvedt (2022), two different approaches were discussed and simulated, involving a curved trajectory and a straight line from the initial placement to the docking receiver.

However, both approaches had limitations, and following a curved trajectory at low velocities and under the influence of disturbances can be challenging for underactuated vessels. To address this issue, the docking approach adopted in this thesis will be similar to the one used by Paris passenger ferries, consisting of four phases: approach turning point, turning, mating the hitch with the receiver, and ensuring that the vessel is docked securely alongside the pier.

The vessel will be in transit mode until it reaches the docking area, at which point it will approach a designated turning point. Once at the turning point, the vessel will rotate until ψ aims directly at the docking receiver. The next step involves moving the hitch towards the receiver, or at least in front of it, to allow for the hitch to slide into place. Upon connecting the docking adapters, a negative yaw moment will be applied to rotate the vessel's aft towards the pier and secure it in place. An illustration of the full routine from transit to docked is shown in Figure 4.1.

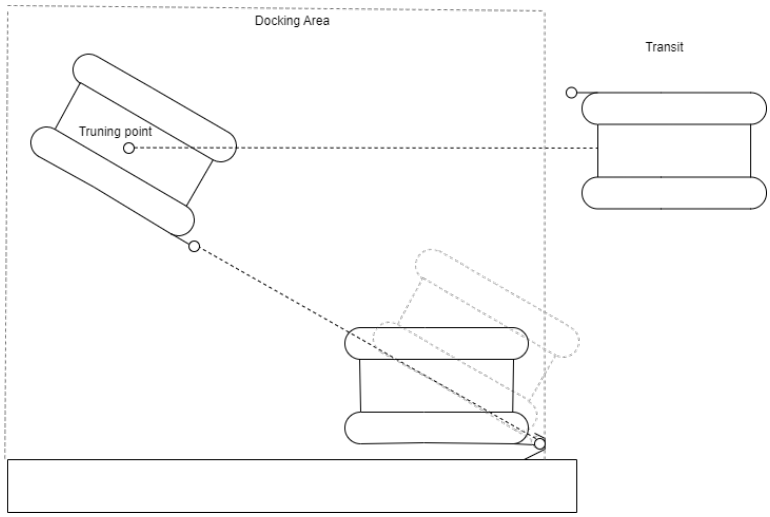

Figure 4.1: The vessel arrives from transit into the docking area, approaches the turning point where it turns, and finally mates the hitch into the receiver (dashed grey) and rotates the vessel's aft into the pier.

4.2 Control overview transit and docking

In this section, the guidance and navigation scheme for the transit and docking routine will be presented. The complete control overview will be depicted in Figure 4.2, followed by a description of the various components within the control overview.

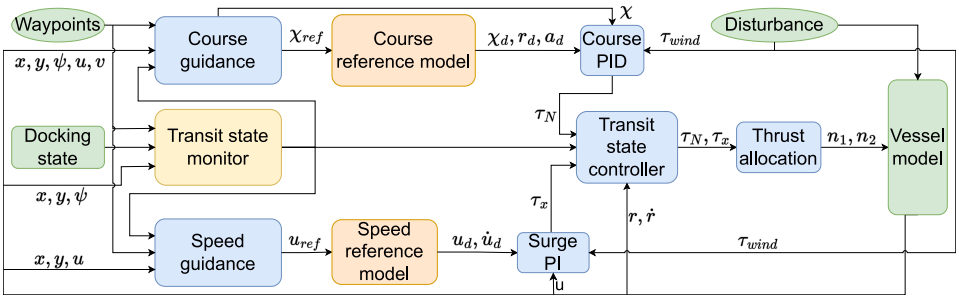

Figure 4.2: Guidance, navigation, and control pipeline utilized in the simulations. The course and speed guidance vary for each state, and the yellow box accurately tracks the current state of the vessel and is illustrated in Figure 4.3.

- **Waypoints** are defined by the user. The waypoints are split into three; first, all the transit waypoints the vessel has to follow to get into the docking area, then there is a turning point, and finally the docking location.
- **Docking state** tells if the vessel is in contact with the docking receiver, the pier, or neither.
- **Course guidance** decides what kind of course guidance the vessel uses according to which state the vessel is in.
- **Transit state monitor** tracks what state the vessel operates in.
- **Course reference model** makes sure that there are no jumps in the course reference signal given to the Course PID.
- **Speed reference model** makes sure that there are no jumps in the speed reference signal given to the Speed PI.
- **Course PID** is a PID controller to make sure that the vessel follows the course reference.
- **Surge PI** is a PI controller to make sure that the vessel holds the speed reference.
- **Transit state controller** is there to make sure that the correct input is given to the thrust allocation. This controller can overwrite the Course PID and Surge PI if the vessel is close to or in touch with the docking point.
- **Thrust allocation** uses the τ_N and τ_x to calculate the correct input for the thrusters
- **Disturbance** is the disturbance given by the wind
- **Vessel model** is the model of The Otter

4.2.1 Transit state monitor

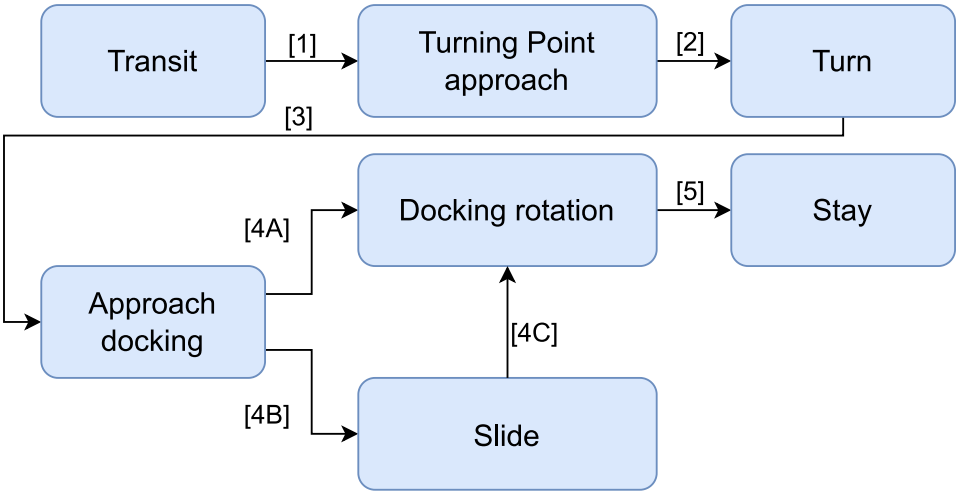

Figure 4.3: Transit state monitor that determines whether the vessel should progress to the next state based on specific conditions within brackets [] assigned to each state and tracks what state the vessel is in.

The transit state monitor requires specific conditions to be met for it to transition from one state to another. These conditions are represented by the numbers inside the brackets in Figure 4.3. The purpose of the state monitor in this thesis is to track the vessel's state while it is in transit until it is fully docked. To transition from the Transit state to the Turning Point Approach state, the condition [1] must be satisfied. Condition [1] is met when the vessel is inside the docking area. The Turning Point Approach state continues until condition [2] is met. Condition [2] is satisfied when the vessel is within a specified radius $r_{turning}$ of the turning point, which is

$$r_{turning} = \sqrt{(\text{vessel}_\text{x} - \text{turning}_\text{x})^2 + (\text{vessel}_\text{y} - \text{turning}_\text{y})^2}, \tag{4.1}$$

where vessel and turning is the vessel's position and the turning point in NED. Once condition [2] is met, the vessel enters the Turn state, which continues until condition [3] is satisfied, which is when the vessel is pointed toward the docking receiver. The docking receiver's direction is given by (4.3). When $|\psi - \text{docking\_direction}| < 1$, [3] is fulfilled. In the Approach Docking state, the state can transition to two different scenarios. The first scenario, called Slide, where the hitch slides along the pier into the docking receiver. To enter this state, condition [4B] must be satisfied, which is achieved when the hitch touches the pier. When the hook connects with the receiver, conditions [4A] and [4C] are fulfilled, and the vessel enters the Docking Rotation state. Finally, when the vessel's side hits the pier while the hook is mated with the receiver, condition [5] is satisfied.

4.2.2 Course guidance

Transit

The course guidance is different for different states and does therefore have the Transit state monitor as input in Figure 4.2. During the transit phase, path following is a commonly used guidance method. When employing path following, the vessel concentrates solely on maintaining the desired path and disregards time or similar factors. Predefined waypoints generate the path. In this thesis, LOS guidance is used. When the vessel transition from Transit, the Docking phase begins.

Docking

To ensure a direct path to the turning point, the angle between the vessel and the turning point is used as the desired course

$$\chi_{\text{ref}} = \text{atan2}(\text{turning\_y} - \text{vessel\_y}, \text{turning\_x} - \text{vessel\_x}). \tag{4.2}$$

This approach eliminates the need for an initial starting point, allowing for an efficient and streamlined navigation process. For the Turn state $\tau_{\text{N}} = -100\text{N}$ making the vessel rotate counterclockwise towards the pier.

During the Approach docking state, the Course guidance does not employ the LOS guidance algorithm. This decision is based on the fact that utilizing the LOS algorithm may lead to the vessel taking unnecessary control actions in order to minimize the cross-track error. The LOS algorithm is primarily designed for path following, ensuring that the vessel remains on the correct path between two waypoints. However, in this thesis, the emphasis lies more on traveling toward the waypoint itself rather than strictly adhering to the direct path. Instead, to determine the course, the angle between the docking hitch and receiver is directly utilized

$$\chi_{\text{ref}} = \text{atan2}(\text{docking\_y} - \text{hitch\_y}, \text{docking\_x} - \text{hitch\_x}), \tag{4.3}$$

where docking and hitch are the docking receiver's and hitch's position in NED. To make sure that the aft does not hit the pier before the docking hitch does, the course reference is

$$\chi_{\text{ref}} = \begin{cases} 95^\circ, & \text{if } \text{d}_{\text{af}} < 1 \text{ and } \psi < 90^\circ \\ \chi_{\textbf{ref}}, & \text{otherwise} \end{cases} \tag{4.4}$$

where d_{af} is the distance between aft and pier. In the first case, ψ is used instead of χ in the PID. This is also done when the distance between the docking hitch and receiver is less than 80cm, to rotate the boat towards the receiver.

4.2.3 Speed guidance

Transit

In the Transit state, $U_{ref} = 1m/s$.

Docking

For the Approach Turning point state, the speed guidance is the same as in Transit. For the Turn state $u_{\text{ref}} = 0$m/s. When the vessel is in Approach docking, $u_{\text{ref}} = 0.7$m/s until it is 5m away from docking then

$$u_{\text{ref}} = \frac{d_{docking}}{10}\text{m/s}, \tag{4.5}$$

where

$$d_{docking} = d_{adapters} + 1, \tag{4.6}$$

where $d_{adapters}$ is the distance between the docking receiver and the docking hitch. The distance is added with 1 to secure that the velocity reference never becomes completely zero when the receivers are close to each other.

4.2.4 Transit state controller

As long as the vessel is not in contact with the pier or docking receiver, the moment and force given by the Course PID and Surge PI will be forwarded to the Thrust allocation. However, as soon as the vessel is in contact with either the pier or docking receiver, the moment and force are overwritten. A docking state input is used to decide what kind of docking state the vessel is in. This can be determined through various means, such as quay contact detection (Helgesen et al., 2022) or estimating the berthing state (Hu et al., 2022). This thesis defines the docking state based on the contact forces present between the vessel and the docking receiver, as well as the pier. The docking states are divided into three distinct states: contact, docking, and fully docked. The contact state occurs when the docking hitch is in contact with the pier, while docking is achieved when the docking hitch successfully connects with the docking receiver. Finally, the fully docked state is attained when the docking hitch is connected to the receiver, and the vessel's side is also in contact with the pier. If the vessel enters Slide state, τN $= 0N$, and τx $= 10N$ to slide the hook into the receiver, and τx $= 10N$ are contained for the rest of the states. Once the docking adapters are securely connected, a negative yaw moment is applied to rotate the vessel towards the pier.

The negative yaw moment was first tried to be a linear function decided by wind speed and direction.

$$\tau_{\text{N}} = c \cdot \text{V}_{\text{w}}, \tag{4.7}$$

where the constant c was obtained by measuring the required moment to rotate the vessel in the simulator under the most intense wind condition in the simulator of 7m/s; subsequently, a lookup table was generated to assign the appropriate c value to the corresponding wind direction. Although this method proved effective in certain scenarios, it was not applicable for all wind directions, particularly when the wind was blowing parallel to the pier towards the docking receiver. As the vessel rotated and moved closer to becoming parallel with the wind, the necessary yaw moment decreased. This means that the vessel needs a different amount of moment to rotate during different parts of the docking rotation. Consequently, the vessel's yaw rate increased significantly before approaching the pier.

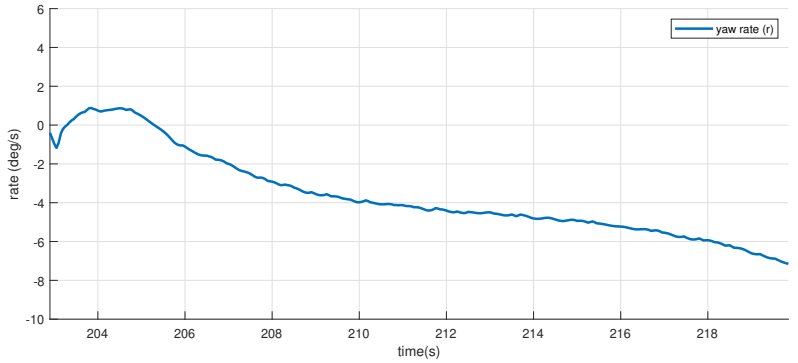

Figure 4.4: The yaw rate during the docking rotation with a constant moment applied. The yaw rate increases even if the moment is constant because of the angle between the vessel and the wind changes. The wind speed is 7m/s, and the wind direction is parallel with the pier in this case.

As depicted in Figure 4.4, the initial moment needed to rotate the vessel generates a yaw rate of roughly $8\,^{\circ}/\mathrm{s}$ upon contact with the pier. This suggests that the rotation should be regulated. To achieve greater precision in managing the impact rate, a PID controller is implemented

$$\tau_{\mathrm{N}} = -\mathrm{K_p}\tilde{\mathrm{r}} - \mathrm{K_d}\dot{\tilde{\mathrm{r}}} - \mathrm{K_i}\int_0^t \tilde{\mathrm{r}}(\tau)\mathrm{d}\tau, \tag{4.8}$$

where $\tilde{\mathrm{r}} = \mathrm{r} - \mathrm{r_{ref}}$, and $\mathrm{K_p}$, $\mathrm{K_d}$, $\mathrm{K_i}$ is the control parameters that need to be tuned.

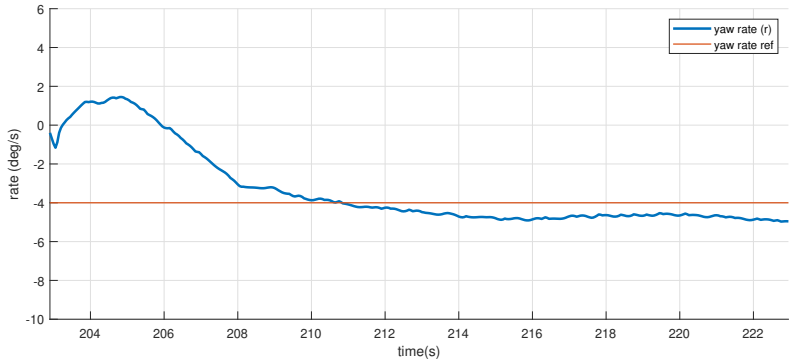

Figure 4.5: The yaw rate of the vessel during the time between the hitch being connected to the receiver and when the vessel is fully docked when the wind speed is 7m/s, and the wind direction is parallel with the pier. A PID controller controls the yaw moment.

The yaw moment is regulated by a PID controller in Figure 4.5 and is exposed to the same wind conditions as in Figure 4.4 and achieves a reduced impact rate which is better.

To make sure that the vessel does not rotate away from the pier during the docked state, the vessel applies a small negative yaw moment. This gives τ_N = -30N.

4.2.5 Course reference model

To ensure a smooth reference to the course controller, reference models can be employed when the course guidance gives sudden changes in courses. The reference model χ_d is based on the commonly selected attitude reference model η_d (Fossen, 2021). Typically, η_d is a third-order model and is constructed from a first-order low-pass filter cascaded with a mass-damper-spring system which gives the transfer function

$$\frac{\chi_d}{\chi_r}(s) = \frac{\omega_n^3}{s^3 + (2\zeta + 1)\omega_n s^2 + (2\zeta + 1)\omega_n^2 s + \omega_n^3}. \tag{4.9}$$

The reference is of third order to ensure continuous steps in χ_d, r_d, and a_d. Incorporating the physical constraints of a craft into the reference model can enhance its performance. Especially it is advantageous to limit the yaw rate $|r_d| \leq r^{max}$ and yaw acceleration $|\dot{r_d}| = |a_d| \leq a^{max}$. This can be done by including saturating elements for yaw rate and acceleration in the reference model (Van Amerongen, 1984). The resulting state-space model is (Fossen, 2021)

$$\dot{\chi_d} = sat(r_d), \tag{4.10a}$$

$$\dot{r_d} = sat(a_d), \tag{4.10b}$$

$$\dot{a_d} = -(2\zeta + 1)\omega_n sat(a_d) - (2\zeta + 1)\omega_n^2 sat(r_d) + \omega_n^3(\chi_r - \chi_d), \tag{4.10c}$$

where

$$sat(x) := \begin{cases} sgn(x)x^{max}, & \text{if } |x| \geq x^{max}. \\ x, & \text{else} \end{cases} \tag{4.11}$$

4.2.6 Velocity reference model

Velocity is of one order higher order than course and needs a second-order low-pass (LP) filter to avoid steps in the velocity reference

$$\frac{u_d}{u_{ref}}(s) = \frac{\omega_{n,u}^2}{s^2 + 2\zeta_u\omega_{n,u}s + \omega_{n,u}^2}, \tag{4.12}$$

since this reference model is of second order, the velocity u_d and the acceleration $\dot{u_d}$ are continuous, while a step in u_{ref} will result in a step in the jerk $\ddot{u_d}$. The state-space representation of (4.12) is

$$\dot{u_d} = \dot{u_d}, \tag{4.13a}$$

$$\ddot{u_d} = -\omega_{n,u}^2 u_d - 2\zeta_u\omega_{n,u}\dot{u_d} + \omega_{n,u}^2(u_{ref} - u_d). \tag{4.13b}$$

4.2.7 Course PID-controller

The course's reference model (4.10) provides continuous steps in χ_d, r_d, and a_d, which is fed into a PID-controller

$$\tau_N = -\tau_{\text{wind}}(I_z - N_{\dot{r}})a_d + N_r r_d - K_p ssa(\chi - \chi_d) - K_d\dot{\tilde{\chi}} - K_i\int_0^t \tilde{\chi}\mathbf{d}\tau, \tag{4.14}$$

to get the desired yaw moment. τ_{wind} is the reference feedforward term and cancels the wind term in yaw, I_z is the inertia about z, $N_{\dot{r}}$ is from the added mass matrix M_A, N_r is calculated due to hydrodynamic derivatives, $\tilde{\chi} = \chi - \chi_d$ and ssa is a function that ensures the smallest difference between two angles (Fossen, 2021). The first two terms are for reference feedforward. The lateral velocities are assumed slowly varying so $\dot{\chi} \approx \dot{\psi}$.

4.2.8 Surge PI-controller

The surge controller employed is a PI-controller, since the vessel typically travels in straight lines between docks, resulting in negligible v in comparison to u. Therefore, the approximation $U = \sqrt{u^2 + v^2} \approx u$ is used, and gives

$$\tau_X = -\tau_{\text{wind}} + d_{11}u_d + m_{11}\dot{u}_d - K_p\tilde{u} - K_i \int_0^t \tilde{u}\mathbf{d}\tau, \tag{4.15}$$

where τ_{wind} is the reference feedforward term and cancels the wind term in surge, $\tilde{u} = u - u_d$, m_{11} is the mass, d_{11} is the damping element in surge, and they are accounted for with reference feedforward.

4.3 Undocking routine

The purpose of the undocking procedure is to allow the vessel to move away from the dock and commence transit in a safe manner. The initial step involves rotating the aft of the vessel away from the pier, after which the vessel begins to travel in reverse. Once the vessel has attained a safe distance from the pier, it steers towards the first transit point and ultimately approaches it. The sequence is illustrated in Figure 4.6.

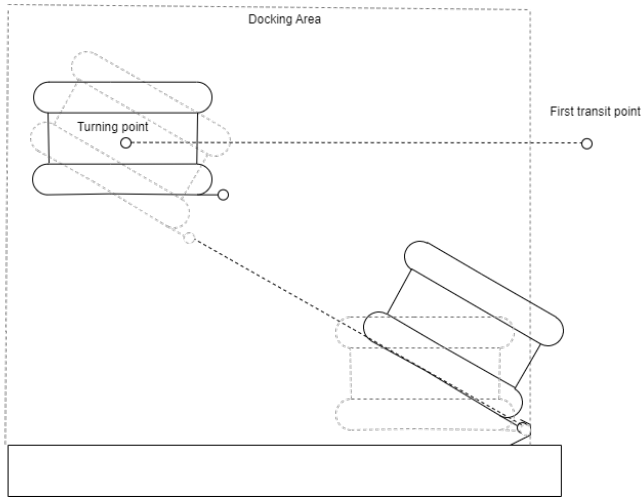

Figure 4.6: The undocking sequence begins with the vessel in a docked position (represented by dashed grey along the pier). Subsequently, the vessel rotates in the receiver until it achieves a certain angle in relation to the pier. Following this, it reverses to a safe distance from the pier (indicated by dashed grey at the turning point). The vessel then rotates towards the first transit point and ultimately proceeds to approach it.

4.4 Control overview undocking

The control mechanisms employed for undocking are identical to those utilized for transit and docking, resulting in a comparable control overview. The control overview for undocking is presented in Figure 4.7. The sole dissimilarities from the control outline depicted in Figure 4.2 are the distinct state monitor and state controller in use. Since the state monitor is different, the course and speed guidance is a bit different as well.

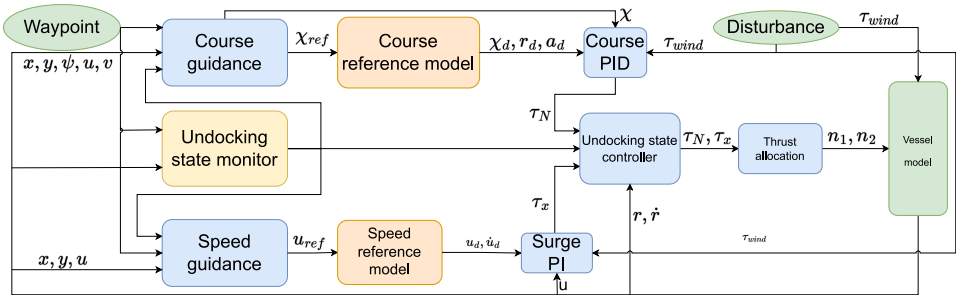

Figure 4.7: The control overview which is quite similar to the one for transit and docking. The State monitor and state controller are different.

- **Waypoint** is the first transit waypoint.
- **Undocking state monitor** tracks what sequence of the undocking routine the vessel is in.
- **Undocking state controller** makes the ultimate decision of which input is fed into thrust allocation.

4.4.1 Undocking state monitor

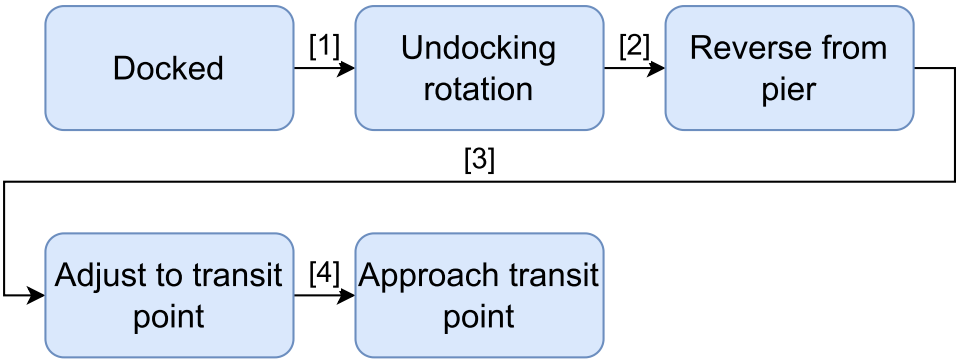

Figure 4.8: The state monitor used for tracking the undocking states.

The purpose of the undocking state monitor is to ensure that the vessel's current stage in the undocking process is identified, and the monitor is described by Figure 4.8. Initially, it is in the docked position until [1] is met, which occurs when an operator initiates undocking or when another signal prompts the vessel to undock. The vessel then begins to rotate until [2] is satisfied, which is achieved when ψ reaches a specific degree. Subsequently, the vessel starts to reverse away from the pier until it reaches a safe distance, [3] is attained when the distance from the pier is safe. Once the vessel has reached a safe distance, it turns towards the transit point until it points in that direction, [4] is reached when the difference between the ψ and the direction towards the first transit point is less than 10°.

4.4.2 Course guidance

As long as the vessel is in contact with the pier, the undocking state controller is in charge of the yaw setpoint and controller. As soon as the vessel begins to reverse, the course reference is

$$\chi_{\text{ref}} = -45°, \tag{4.16}$$

which is 45°away from the pier; when the turning begins, the rotation is the same as in Subsection 4.2.2, $\tau_{\text{N}} = -100\text{N}$. For the approach transit point, the course reference is

$$\chi_{\text{ref}} = \text{atan2}(\text{firstTransit\_y} - \text{vessel\_y}, \text{firstTransit\_x} - \text{vessel\_x}), \tag{4.17}$$

where firstTransit is the first transit point in NED.

4.4.3 Speed guidance

For the reverse from the pier state, the speed reference is $u_{\text{d}} = -0.5\text{m/s}$, while it is 1m/s for the approach transit point.

4.4.4 Undocking state controller

This controller controls undocking rotation. The same PID (4.8) is used for the undocking rotation as in Subsection 4.2.4, with 3°/s as reference.

Chapter 5

Simulation results

In this chapter, simulation results for the methods developed in this thesis are presented, which will include a thorough analysis of the advantages and disadvantages of the developed docking scheme. This thesis also proposes a solution for transit, which is quite similar to the transit solution for fully-actuated vessels. Undocking operation is also developed to get a full dock-to-dock system, but the docking procedure is the most complex. Therefore, the focus of the results will mainly be on the docking outcomes. First, the parameters used in the thesis will be given, then will the total route be given in Section 5.2, the whole route through all the transit points as well as the turning and docking point. In Section 5.3, the undocking results are given, while the transit results are given in Section 5.4.

The results of the docking process are compiled in Section 5.5. Four scenarios have been devised to explore the docking procedure. Initially, the procedure will be executed without any disturbances to assess its performance under calm conditions and serve as a benchmark for comparison with windy conditions. Various criteria will be employed to evaluate the docking process, including impact velocity, impact point, impact angle, time taken from contact to complete docking, docking time, and metrics for the surge and course controllers. The second scenario will assess the same criteria while docking under different wind speeds and directions. The third scenario will focus on investigating the wind direction that presents the greatest challenge in the second scenario. Lastly, the fourth scenario will investigate the possibility of improving results for the wind direction examined in scenario three by altering the turning point.

There are videos that show the undocking and docking operation with wind speeds 0m/s, as well as docking operation for different wind speeds and directions at URL:
https://www.youtube.com/@JonasHorntvedt/videos.

5.1 Parameters

Parameter	Value	Description
ρ_a	1.204	Air density
A_{L_w}	1	Lateral projected area
A_{F_w}	1	Frontal projected area
L_{oa}	2	Overall length
K_p	1200	PID docking rotation
K_i	500	PID docking rotation
K_d	300	PID docking rotation
ω_n	1.5	Course reference model
ζ_n	1.0	Course reference model
ω_n	1.6	Surge reference model
ζ_n	1.5	Surge reference model
K_p	272.5	PID course controller
K_i	52.93	PID course controller
K_d	190.1	PID course controller
K_p	$m_{11} \cdot \omega_n^2$	PI surge controller
K_i	$\omega_n \cdot 0.1 \cdot K_p$	PI surge controller

Table 5.1: Parameters used in the thesis

C_X, C_Y and C_N are calculated using blendermann94.m in the MSS toolbox (Fossen, 2022), with passenger liner as the chosen vessel. The surge controller's parameters are given by the PID algorithm in Fossen (2021).

5.2 Route

The thesis has created controllers specifically designed for autonomous vessels navigating through waypoints, with the vessel following a path defined by the waypoints in order. Starting in the Transit state at $p_{starting} = [100, 100]$, the vessel will navigate through the transit waypoints

$$\text{transit\_x} = \begin{bmatrix} 100 & 50 & 50 & 3 & 8 \end{bmatrix}$$

$$\text{transit\_y} = \begin{bmatrix} 100 & 80 & 50 & 25 & 10 \end{bmatrix}$$

until it reaches the docking area, where $y < 10$. Once inside the docking area, the vessel will set a course for the turning point $p_{turning} = [12, -12]$, $r_{turning} = 2$m, turn, and proceed towards the final docking point $p_{docking} = [0, 0]$. Upon successfully reaching $p_{docking}$, the vessel will rotate its side towards the pier to finalize the docking procedure. The full route is shown in Figure 5.1.

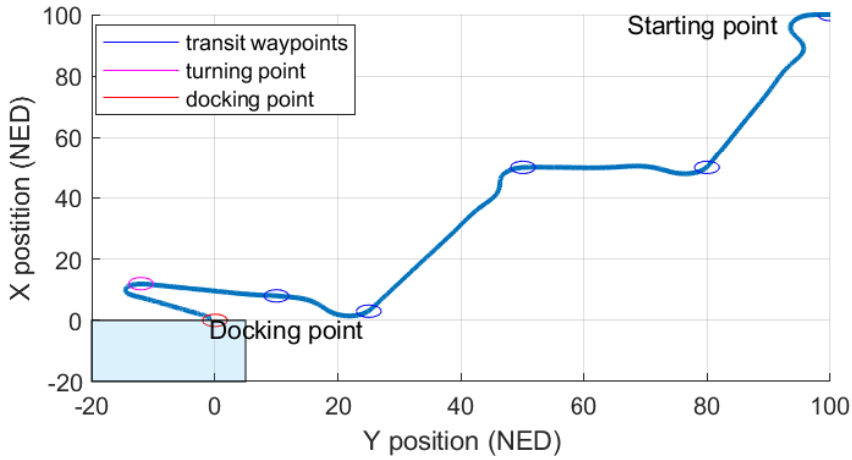

Figure 5.1: The full route the vessel travels from $p_{starting}$ to $p_{docking}$ through $p_{turning}$.

While the states and thrust during the full sequence is presented in Figure 5.2 and Figure 5.3.

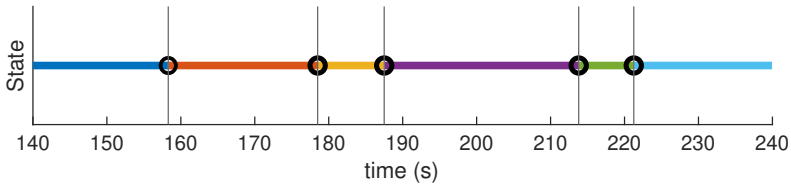

Figure 5.2: The states during the full route. Remark that the plot starts after 140s, it is in transit for t $\in$ [0,157.1], the blue line. The second state is the Turning point approach, the orange line. The third state is the Turn state, the yellow line. The fourth state is the Approach Docking state, the purple line. The fifth state is Docking rotation and slide state, the green line. The final state is the Stay state which says the vessel is fully docked, the turquoise line.

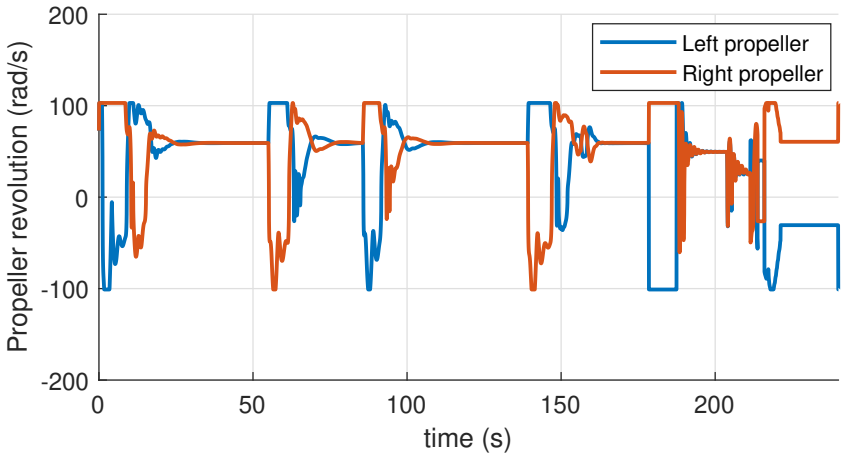

Figure 5.3: The propeller revolutions during the full route, from $p_{starting}$, to fully docked. Remark that the maximum rad/s is 103, and the minimum rad/s is -101 for The Otter.

5.3 Undocking results

As the thesis does not primarily focus on undocking, the results will not be subjected to an in-depth analysis. However, the findings will include the undocking operation up to the first transit point for wind speed 7m/s in all wind directions. The vessel rotates until $\psi > 135°$, which makes an angle of 45°between the pier and the vessel. Then the vessel reverses until it is 2.5m away from the pier. The final sequence includes rotating the vessel towards the transit point and finally approaching it.

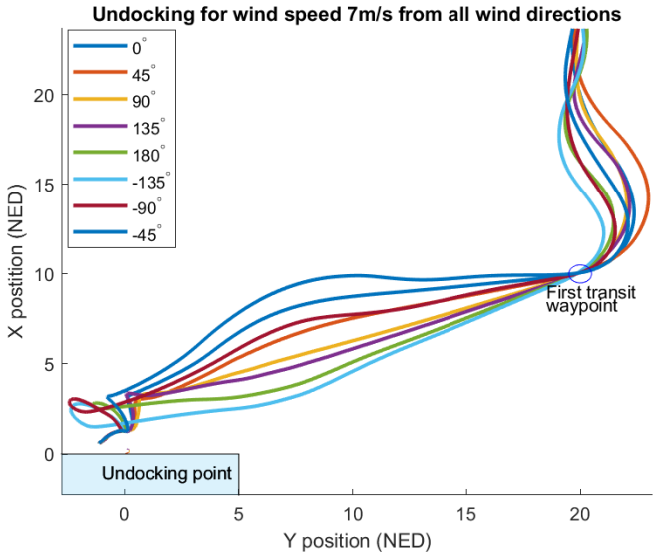

Figure 5.4: The undocking operation for all wind direction and wind speed 7m/s. The vessel undocks at $p_{docking}$, turns toward the transit point when the distance to the pier is 2.5m, then travels to $wp_1 = [10, 20]$

As demonstrated in Figure 5.4, the vessel effectively executes the undocking operation. Although there are variations in the trajectories, the vessel maintains a secure distance from the pier in all scenarios and ultimately reaches the waypoint.

5.4 Transit results

The findings will depict the transit trajectories for wind speeds up to 7m/s in all wind directions.

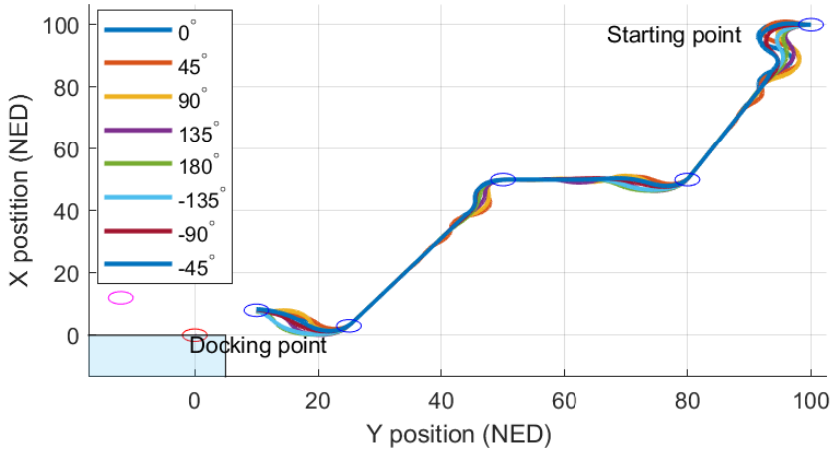

Figure 5.5: All vessel trajectories when experiencing 7m/s for each wind direction. The vessel travels from $p_{starting}$ to p_{ending}.

As evidenced by Figure 5.5, the vessel can successfully reach all waypoints along the transit route. Although the trajectories may vary slightly between waypoints, the vessel manages to track the transit path successfully regardless of the wind direction.

5.5 Docking results

Although a vessel coming to a complete stop next to the pier can be considered successful docking, specific criteria can be evaluated to assess the quality of the achieved docking.

- **Impact velocity** of the vessel will be assessed to determine the force with which the vessel collides with the pier or docking receiver. The impact velocity is U_{impact}, and the impact surge will be examined as well and is u_{impact}.
- **Impact point** is how far off the receiver the hitch hits and will be examined to compare how the different wind speeds and directions influence the impact point. The impact point is p_{impact}.
- **Impact angle** refers to the angle formed between the heading of a vessel and the pier at the moment of impact and is given by α_{impact}. Assuming the pier is oriented

towards the east (at 90 degrees), the impact angle can be calculated as $\alpha_{impact} = \psi - 90$. It's important to note that a successful docking process should aim to minimize the impact angle, as larger angles will require more docking rotation after impact and hence an increased docking time.

- **Time between Impact to fully docked** will be analyzed to evaluate the efficiency of each approach and the influence of impact point on time to completed docking. Impact time is defined T_{impact} and time to completed docking is T_{docked}.
- **Docking Time** will be analyzed to see if the docking scheme gets more inefficient for stronger winds. The docking time is $T_{docking}$.
- **Surge and course metric** will be evaluated to see how well the controller follows the desired course and speed set points. This can tell if the docking is pure luck or if it is safe and follows the given set points. The metrics are constructed to penalize the error more when closer to docking because this is the most critical phase. The metric for the course is

$$metric = metric_{previous} + \frac{1}{d+1}|\chi_d - \chi|, \tag{5.1}$$

where metric$_{previous}$ is the last value of metric and d is the distance to docking. The metric for the surge is similar to (5.1). The metric will only be calculated during the approach docking state.

In order to assess the effectiveness of the docking scheme, various scenarios will be utilized to test the vessel. This will help to determine the robustness of the scheme and its overall effectiveness.

- **Scenario 1** will investigate how well the docking scheme works without disturbance.
- **Scenario 2** will involve evaluating the docking scheme under a range of wind speeds and directions. The wind will be directed from angles spanning from -180°to 180°relative to the north, with increments of 25°. The wind speeds will be in the span of 0-7m/s with increments of 0.1m/s. The assessment will include an analysis of the average and maximum values of the specified criteria for each scenario.
- **Scenario 3** will investigate the wind direction that presents the greatest difficulty for the docking scheme.
- **Scenario 4** will investigate if it is possible to tune the docking scheme to improve the docking for the wind direction used in Scenario 3.

5.5.1 Scenario 1

Figure 5.6 displays U observed during the final moments of the docking process. As indicated by the graph, the resulting $U_{impact} = 0.16m/s$. It was expected that without

any wind disturbance, U_{impact} would be good. The vessel's speed controller is based on u, and without any wind, the lateral velocities are really small, so $u \approx U$. Such a low velocity is considered ideal since it will not cause any discomfort for the passengers. Therefore, the observed U_{impact} aligns with the desired outcome.

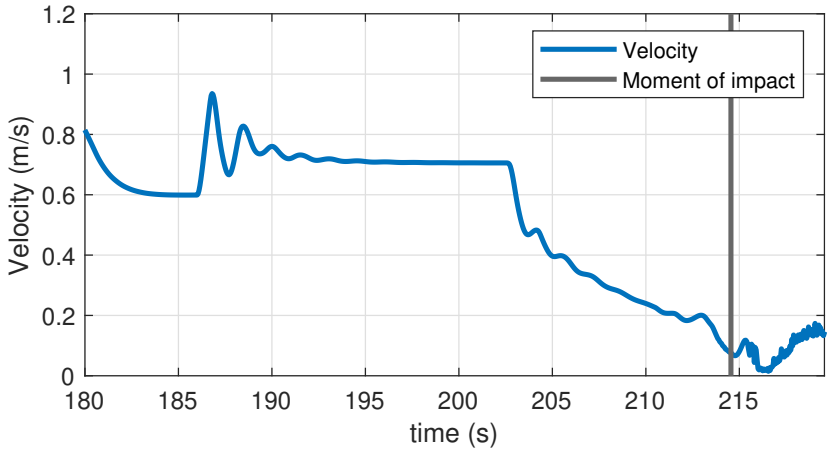

Figure 5.6: Scenario 1: U in the final seconds before and right after impact with the pier or receiver.

After the impact, U is still non-zero, which can be attributed to ongoing adjustments required for the vessel to dock successfully. Initially, the vessel slides into the receiver and subsequently rotates, with the velocity component v playing a role in generating a non-zero value for U.

In order to accurately determine the location of the p_{impact}, an investigation of the docking hitch's position in the NED coordinate system during the time of impact is essential. This analysis allows to effectively assess where the docking hitch comes into contact with the docking receiver.

Figure 5.7 displays y of the docking hitch in NED coordinates during impact. As depicted in the graph, at the moment of impact, $y = -0.20$. This information, when combined with the y in $p_{docking}$ is 0, it is possible to precisely pinpoint the location of p_{impact}. Based on the data gathered from the graph, it can be seen that p_{impact} is situated 0.2m ahead of the docking receiver. That the boat needs to slide 20cm is a good result and validates the course controller works well without any disturbance.

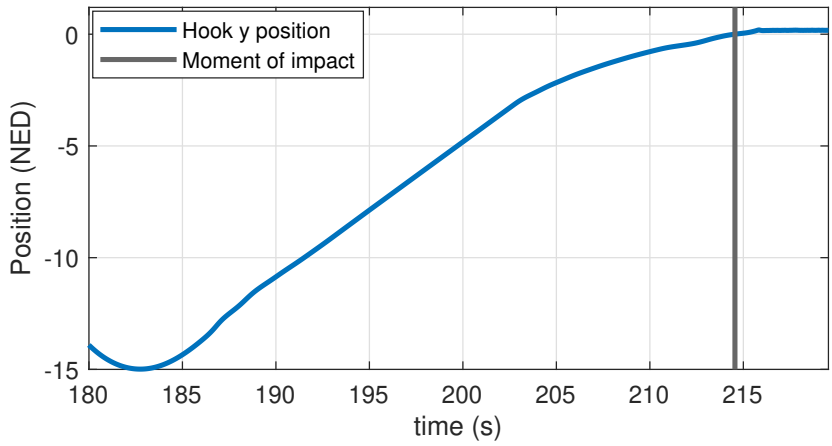

Figure 5.7: Scenario 1: The docking hitch's y position in NED during the final seconds of the docking, including the time of impact.

The heading, ψ, during the approach docking state is shown in Figure 5.8. The graph indicates that the vessel maintains a ψ of 117.36°at T_{impact}, resulting in $\alpha_{impact} = 27.36°$. This angle is favorable for docking as it suggests that the vessel does not require significant rotation to complete the docking process. Given that the turning point is positioned at 45 degrees relative to the pier, any α_{impact} close to or less than 45°can be regarded as satisfactory.

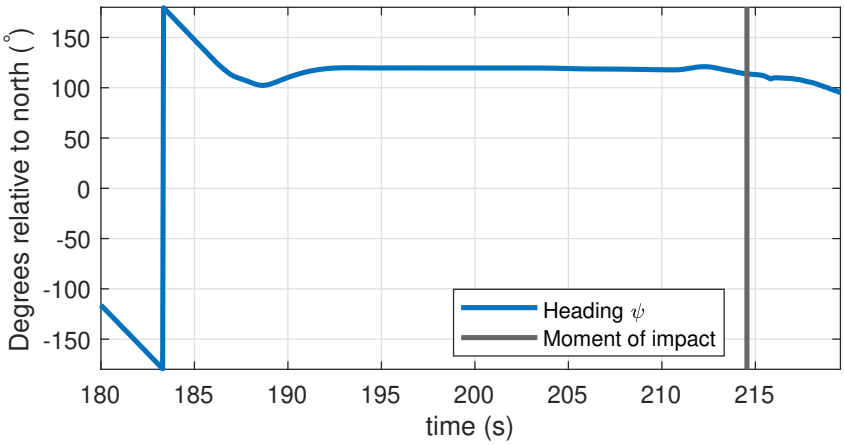

Figure 5.8: Scenario 1: ψ during the approach docking state, and T_{impact}.

In Figure 5.9, all possible docking states, including the fully docked state, are presented.

The docking process involves several stages, starting with the contact state. During this state, the docking hitch is in contact with the pier, but the hitch has not yet connected to the receiver. The docked state is achieved once the hitch slides and connects to the receiver. At this point, the vessel is partially docked, and there is still some adjustment needed to reach the fully docked state.

The fully docked state is attained when the vessel aligns with the pier and its side touches it. In this state, the vessel is completely stable and secure, and all loading and unloading operations can be performed safely.

The contact state appears after t = 213.6 s. The docked state is achieved after 215.4 s, suggesting that the hitch has successfully connected to the receiver and the vessel is partially docked.

The vessel reaches the fully docked state in 221.2 s, indicating that it takes approximately 5.8 s for the hitch to rotate and secure the vessel in place. The elapsed time between impact and the fully docked state is 7.6 s, which is relatively short and can be considered a favorable outcome.

It's worth noting that if the hitch directly hits the receiver, the contact state would not be present, so $T_{impact} = T_{docked} + T_{slide}$. However, in the current docking process, the hitch must slide and adjust its position before rotating and securing the vessel.

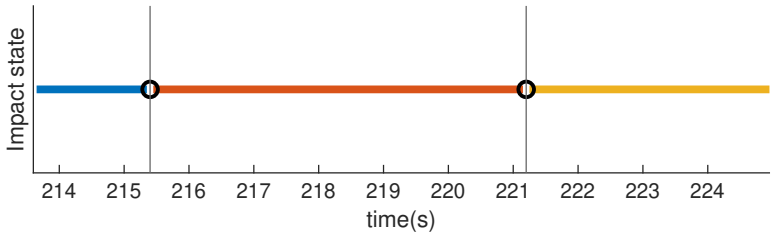

Figure 5.9: Scenario 1: The time span where the docking hitch first hits the pier, blue line, and then slides into the receiver. Finally, the hitch is mated with the receiver, orange line, until the fully docked state is achieved, yellow line, as the vessel's side is in contact with the pier while the docking adapters are connected. The plot starts in the transition between the approach docking state and contact with the pier.

Due to this being the first use of the course metric, there is some uncertainty regarding the accuracy of the results. Nevertheless, it is reasonable to assume that the metrics will best results when the wind is not present. To see if the course controller performs well, it will be necessary to supplement the findings of the course and the desired course in Figure 5.11. Later the value obtained from this metric can be compared with those acquired from tests that were impacted by wind. Figure 5.10 presents the outcome of the course metric, where it can be observed to be 14.82, which is uncertain if it is good or not.

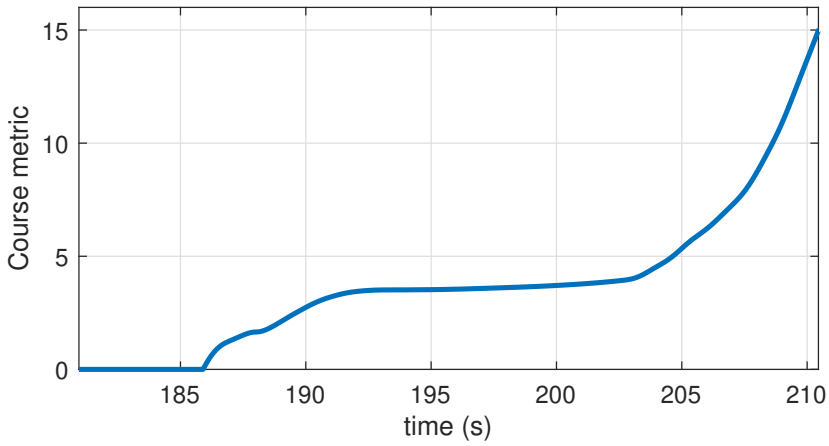

Figure 5.10: Scenario 1: The course metric during the approach docking state

In the approach docking state, Figure 5.11 illustrates the vessel's adjustment towards the intended course. The vessel rotates until the variance between its heading and the direction towards the docking receiver is below 1°. The vessel promptly aligns with the appropriate course and maintains this course toward the receiver. It is clear that the course controller works well in this case, which means that $metric_{course} = 14.82$ is a good result for the course metric.

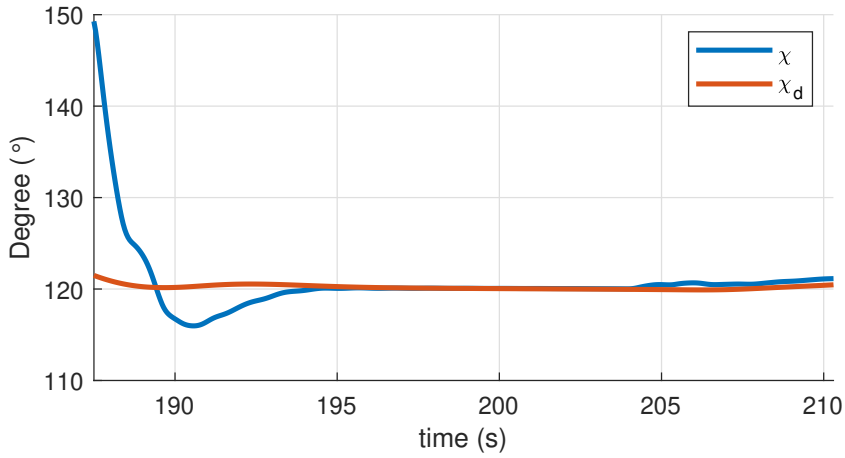

Figure 5.11: Scenario 1: The course and desired course plot during the approaching docking state.

Similar to the course metric, a similar argument for the surge metric can be made. On its own, it may be difficult to determine whether the result is favorable or not. Nevertheless,

the outcome can be used as a point of comparison for future tests that incorporate wind disturbance. In the absence of wind $metric_{surge} = 0.18$, as demonstrated in Figure 5.12.

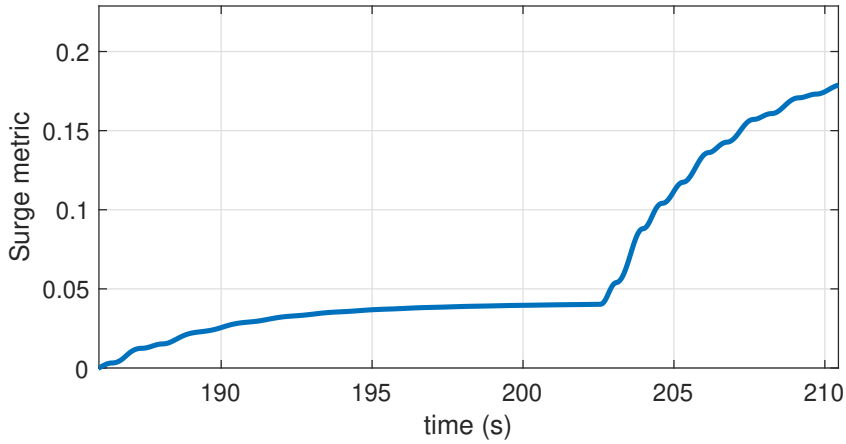

Figure 5.12: Scenario 1: The surge metric during the approach docking state

Figure 5.13 illustrates how U is aligned with u_d during the docking approach state. A reference jump occurs as the vessel transitions from turning to approach docking state. U oscillates briefly before eventually aligning with u_d. Since there are no disturbances in the straight-line path toward the docking receiver, $U \approx u$, which is good since the speed is regulated after u. Once the alignment is achieved, U closely follows u_d towards the docking receiver. Again, a good result and $metric_{surge} = 0.18$ is a good result for the surge metric.

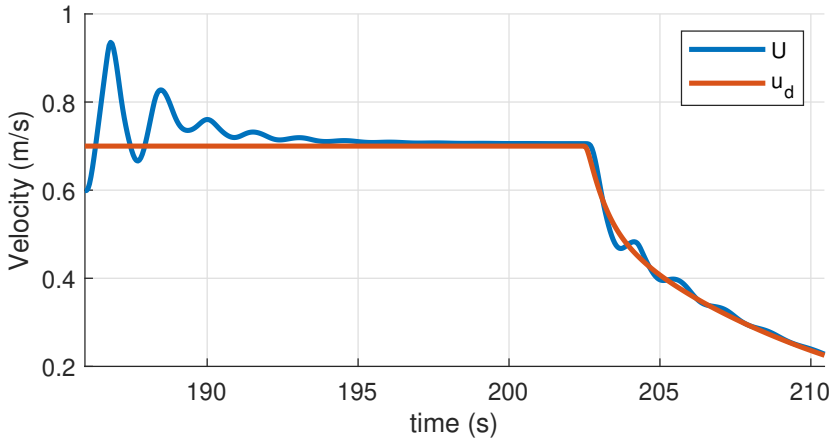

Figure 5.13: Scenario 1: The U and u_d plot during the approaching docking state.

5.5.2 Scenario 2

As the vessel is underactuated, only u is controlled, not U. However, there are differences between the u_{impact} and U_{impact}, as shown in Figure 5.14 and Figure 5.15. This is expected, as the wind can cause sideways velocity, increasing U relative to u.

Concerning u_{impact}, the highest recorded value is 0.38m/s which is deemed uncomfortable for passengers but may be tolerable during extremely challenging circumstances. However, for the remaining simulated wind directions, $u_{impact} = 0.3$m/s, which is satisfactory given that this is the worst-case scenario. In terms of U_{impact}, the findings are unfavorable. The highest recorded value is 0.52m/s, which is considered intolerable as it would cause significant discomfort for passengers. This highlights a limitation in managing the u rather than U. Even if u appears to be within acceptable limits, the contribution of v can still result in an excessive U. Wind direction $\beta_w = -135°$presents the most challenging conditions for u_{impact} and U_{impact}. When approaching the docking receiver, the vessel turns at [12,-12] and $\chi \approx 135°$. Under these circumstances, if $\beta_w = -135°$, it will act perpendicularly on the vessel, resulting in the largest possible u_{impact} and U_{impact}. This is because the boat's side represents its biggest area, and the wind pushes the vessel towards the pier, exacerbating the U_{impact}.

Based on the findings presented in Figure 5.14, it is evident that the most challenging maximum conditions occur when winds blow in a clockwise direction relative to the north between 45° and -135°. This can be explained by the wind blows perpendicularly on the vessel at 45°, making it hard for the controller to follow the reference. Meanwhile, at 90°, the wind comes from behind the boat, resulting in higher speeds. Winds blowing from 135° and 180° both push the vessel towards the pier, further increasing the U_{impact}. In Scenario 3, the maximum U_{impact} will be further investigated.

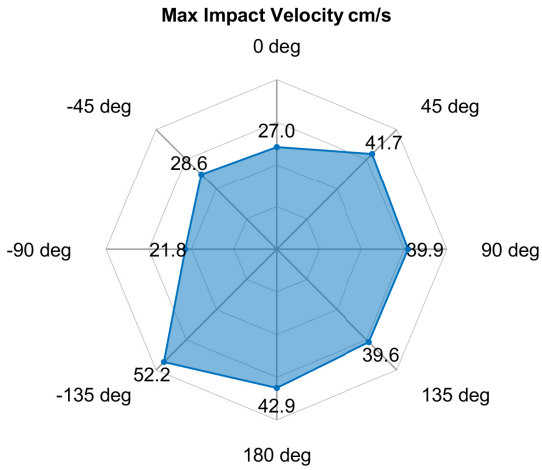

Figure 5.14: Scenario 2: The maximum U_{impact} according to each wind direction.

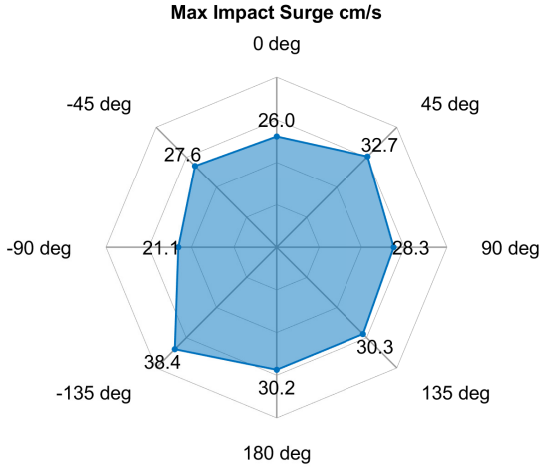

Figure 5.15: Scenario 2: The maximum u_{impact} according to each wind direction.

Wind direction (°)	Wind speed (m/s)
0	0.9
45	7.0
90	6.9
135	6.4
180	6.0
-135	7.0
-90	6.6
-45	3.7

Table 5.2: Scenario 2: A tabular representation indicating the wind speeds at which the maximum U_{impact} is attained for every direction of the wind.

Stronger winds generally lead to higher U_{impact}, as shown in Table 5.2 for almost all wind directions. However, there are exceptions: at 0°, the maximum U_{impact} is achieved at a wind speed of 0.9m/s, and at -45°, the maximum U_{impact} occurs at a wind speed of 3.7m/s. Since both of these winds push the vessel away from the docking, they do not result in a direct increase in U_{impact}. At 45°, the wind also pushes the vessel away from the pier but still achieves the maximum U_{impact} at wind speed 7m/s. This may be due to the fact that the wind hits the vessel perpendicular, resulting in the maximum impact from the wind and potentially causing a larger control error and greater U_{impact}.

To obtain the average result, the mean is computed by 71 values for each wind direction. First, u is examined, as it's the parameter that is controlled. The results obtained are displayed in Figure 5.17, indicating that u_{impact} is quite favorable for the average scenario. Although $\beta_w = -135°$poses the greatest difficulty, the average u_{impact} of 0.22m/s is a highly satisfactory outcome. Moreover, the remaining average u_{impact} are all below 0.2m/s. Likewise, Figure 5.16 depicts the average U_{impact}, which is slightly higher than that for u owing to the lateral velocity component. Nonetheless, the outcomes for the average scenario are quite favorable, and the U_{impact} is not expected to cause any significant discomfort in the average case. These outcomes provide evidence that the most challenging β_w are those in a clockwise orientation relative to north, falling within the range of 45° to -135°.

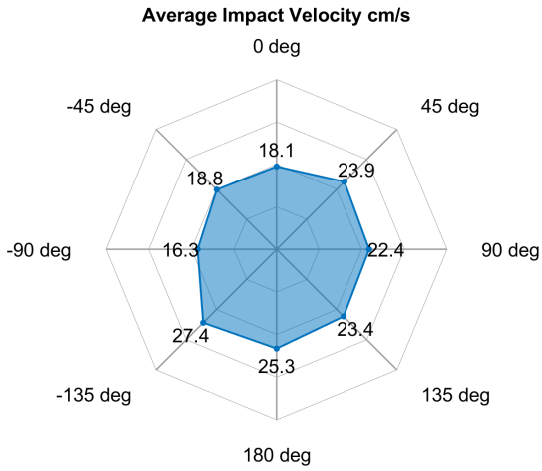

Figure 5.16: Scenario 2: The average U_{impact} according to each wind direction

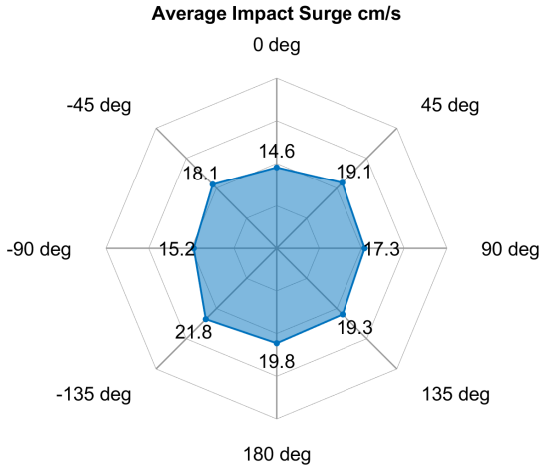

Figure 5.17: Scenario 2: The average u_{impact} according to each wind direction

Based on Figure 5.18, it is evident that the most significant issues arise when the vessel experiences the same conditions that lead to a decrease in U_{impact}. This makes sense given the correlation between p_{impact} and U_{impact}. The velocity is controlled by the distance

to the docking receiver as shown in (4.5). When the vessel hits further away from the docking receiver, u_{ref} will be higher which gives bigger u and U. $\beta_w = -135°$proves to be the most challenging to handle, with a maximum p_{impact} of 1.7m, which means that the vessel must slide 1.7m after impact with the pier, an undesirable outcome. The same is applicable for wind directions of 180 and -135°. Given that these three wind directions all drive the vessel towards the pier, it is logical that they result in the greatest p_{impact}. Moreover, the vessel must aim north/east of the docking receiver to counteract the wind and achieve the appropriate course. This can make the vessel to move towards the pier with ψ aligned with the pier. However, for the remaining wind directions, the maximum p_{impact} is 0.5m, which is satisfactory, given the low-velocity maneuvering in rough winds.

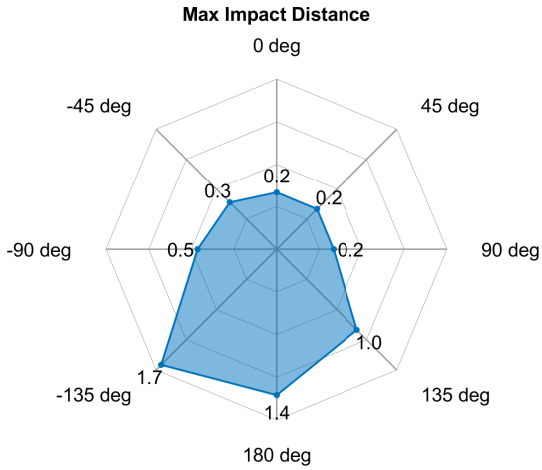

Figure 5.18: Scenario 2: The maximum p_{impact} according to each wind direction

Wind direction (°)	Wind speed (m/s)
0	0.0
45	0.0
90	0.0
135	7.0
180	7.0
-135	7.0
-90	6.7
-45	7.0

Table 5.3: Scenario 2: A tabular representation indicating the wind speeds at which the maximum p_{impact} is attained for every direction of the wind.

Table 5.3 highlights that the majority of maximum p_{impact} occur when the wind speed is between 6-7m/s. Nonetheless, wind directions of 0, 45, and 90°attain their maximum p_{impact} at 0m. This can be attributed to the fact that, during stronger winds, the vessel tends to be pushed away from the pier, resulting in the hitch hitting directly into the docking receiver.

The average p_{impact} for winds blowing in the $\beta_w = -135°$direction is 0.7m, while for $\beta_w = 180°$, it is 0.6m. However, it is not acceptable to miss the docking receiver by an average of 60-70cm. On the positive side, the docking sequence produces good results when the vessel is subjected to the other specified wind directions. The average p_{impact} for winds blowing in the -90 and 135°directions is 0.4m away from the docking receiver, while for the remaining wind directions, the p_{impact} is precisely at the docking receiver.

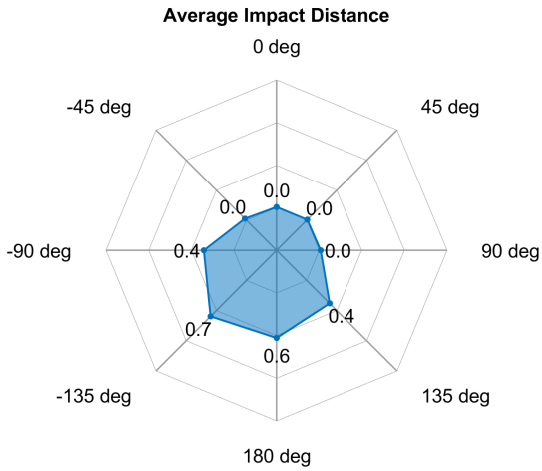

Figure 5.19: Scenario 2: The average p_{impact} according to each wind direction

The impact angle, α_{impact}, is a useful metric for evaluating the effectiveness of a docking scheme. As depicted in Figure 5.20, wind directions of 45 and 90°present the most significant challenges in terms of α_{impact}. It's worth noting that $\alpha_{impact} = 87°$and $\alpha_{impact} = 84.6°$are uncomfortably close to 90°, which could result in almost perpendicular contact with the pier and increase the docking rotation. It is logical that these two wind directions result in the largest α_{impact}, as when the wind is blowing at 45 and 90°, the vessel must aim south/west of the docking receiver to offset the wind and maintain the correct course. Given that the turning point occurs at [12,-12], the ideal impact angle should be approximately 45°or less since this is the angle between the turning point and the docking location. Fortunately, the remaining wind directions tested displayed acceptable maximum α_{impact}, with the highest being 60.8°, which is only 15.8°above the

anticipated angle and thus a manageable worst-case scenario. The results support the observation made during the examination of the impact points, which suggested that winds blowing towards the pier cause the vessel to aim north/east of the receiver to offset the wind as these wind directions have low maximum α_{impact}. This is further supported by the smallest impact angles being observed for these wind directions.

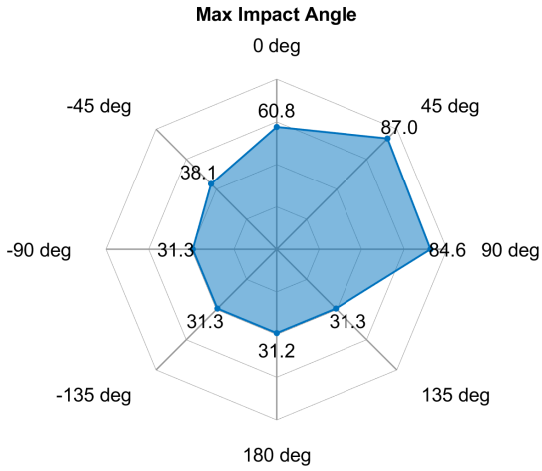

Figure 5.20: Scenario 2: The maximum α_{impact} according to each wind direction

As demonstrated in Figure 5.21, wind directions of 45 and 90 degrees continue to produce the largest α_{impact}, with average α_{impact} of 54.5 and 51.5 degrees, respectively. Given that the anticipated α_{impact} is approximately 45 degrees, an average case with less than 10°errors would be considered satisfactory. Notably, the smallest average α_{impact} of 10.8°is achieved when $\beta_w = -135°$. In this scenario, the docking rotation will be minimal, which is favorable.

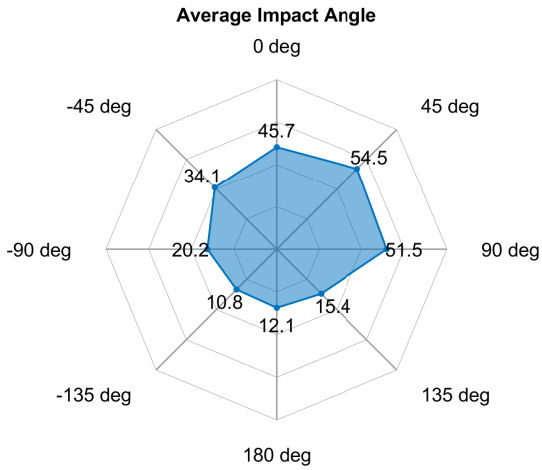

Figure 5.21: Scenario 2: The average impact angle according to each wind direction

The maximum duration between T_{impact} and T_{docked} is displayed in Figure 5.22. The longest maximum time of $23.2\,\mathrm{s}$ occurs when $\beta_w = 45°$, which is slightly longer than desired. Notably, the wind directions of 0, 45, and 90°produce the longest maximum times, which is reasonable as they are perpendicular to the vessel during different phases of the docking rotation. Nevertheless, factors beyond wind, such as impact point and angle, also play a role in determining the docking time. The maximum duration for achieving full docking exhibits a similar trend to the maximum ψ_{impact}, implying that a larger ψ_{impact} results in an extended time required for full docking.

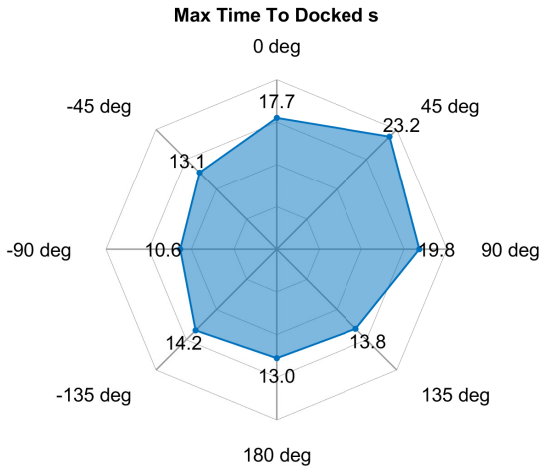

Figure 5.22: Scenario 2: The maximum docking time according to each wind direction

Wind direction (°)	Wind speed (m/s)
0	7.0
45	7.0
90	7.0
135	2.9
180	2.1
-135	1.9
-90	4.4
-45	7.0

Table 5.4: Scenario 2: A tabular representation indicating the wind speeds at which the maximum time to fully docked is attained for every direction of the wind.

The longest time to fully dock is not limited to rough winds, as demonstrated in Table 5.4. When the wind direction is perpendicular to the vessel during the docking rotation in three particular directions, the maximum docking time occurs at maximum wind speeds. The same yields for $\beta_w = -45°$. However, for all other directions, the wind speed ranges from 1.9-4.4m/s. This will be further investigated in the Docking Time criteria.

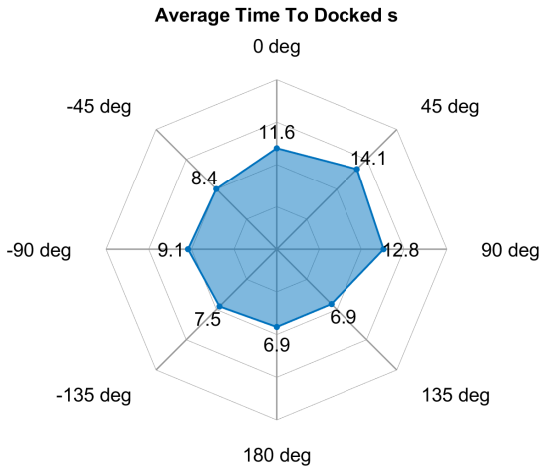

Figure 5.23: Scenario 2: The average docking time according to each wind direction

For the docking time, only the maximum and minimum will be compared to see how much the wind affects the docking time.

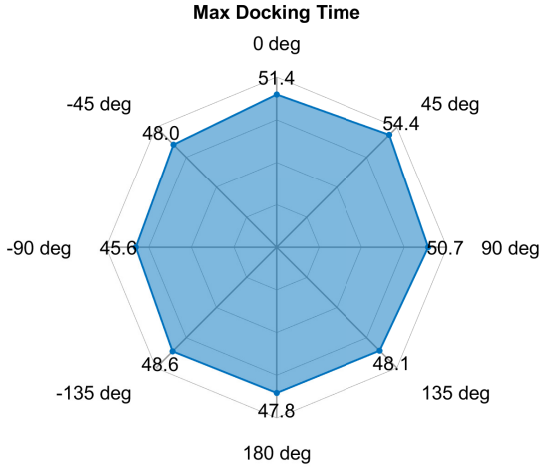

Figure 5.24: Scenario 2: The maximum docking according to each wind direction

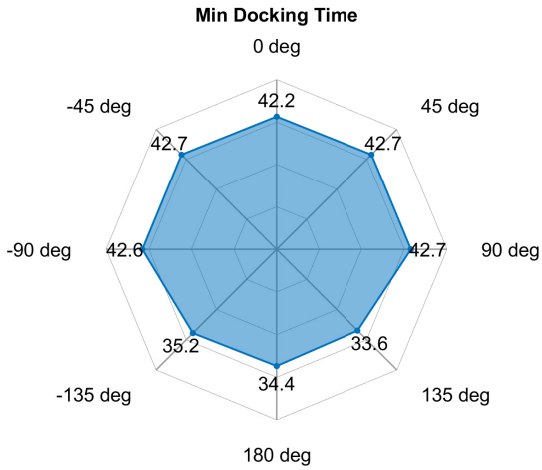

Figure 5.25: Scenario 2: The minimum docking according to each wind direction

The duration required for the vessel to dock fully is referred to as $T_{docking}$, which starts from the initiation of the turning state, and ends when the vessel is fully docked. Figure 5.24 and Figure 5.25 exhibit the maximum and minimum $T_{docking}$ for each wind direction. The outcomes indicate that $\beta_w = 45°$has the highest maximum and minimum values, which is reasonable since the wind will act perpendicular to the vessel at some point during the docking rotation. For $\beta_w = 180°$, this is reduced since the docking rotation already has picked up speed when the vessel is perpendicular to this wind direction. For $\beta_w \in \{-45°, 45°, 90°, 0°\}$, the difference between the maximum and minimum $T_{docking}$ is not significant, ranging from 3 to 8s. However, for $\beta_w = 45°$, the difference is 11.7s, which is reasonable as the docking rotation becomes more challenging in stronger winds. Nonetheless, for $\beta_w \in$ {-135°, 180°, 135°}, the difference between the maximum and minimum docking time exceeds 10s. Considering the results from the p_{impact} and ψ_{impact}, this may be due to the sliding distance for these three wind impact distances. However, it would be reasonable to assume that $T_{docking}$ could be reduced in stronger winds as the wind would push the vessel towards the pier at a faster rate. Therefore, an examination of $T_{docking}$ in relation to wind speeds for these three wind directions will be conducted.

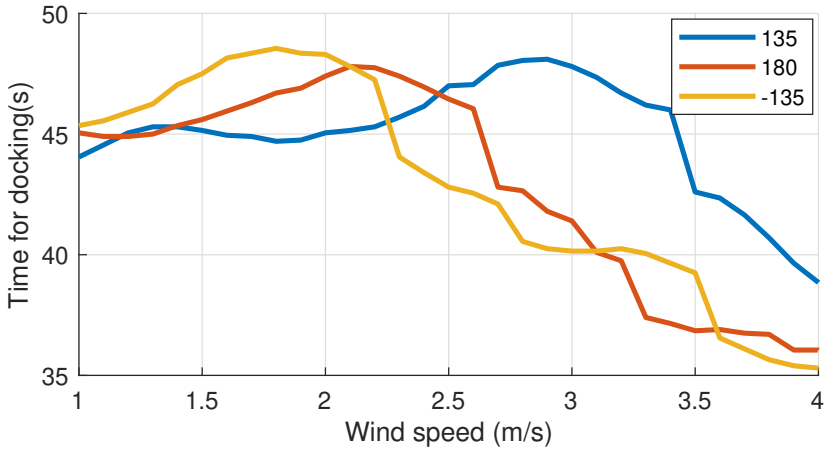

Figure 5.26: Scenario 3: The three wind directions that have the biggest differences between maximum and minimum $T_{docking}$ for all wind speeds.

The $T_{docking}$ for the three distinct wind directions display a similar trend, as illustrated in Figure 5.26. Initially, the $T_{docking}$ increases and then subsequently decreases. To scrutinize this trend, a review of p_{impact} and ψ_{impact} combination will be conducted.

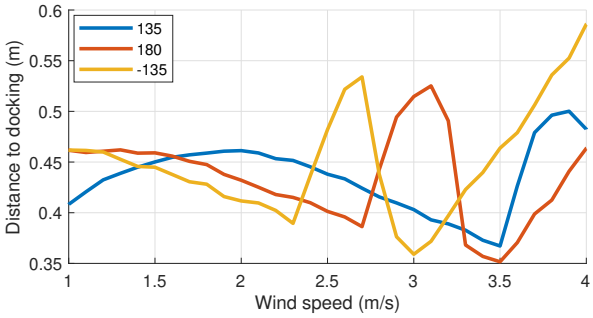

(a) Scenario 3: The three wind directions that have the biggest differences between maximum and minimum $T_{docking}$ for all wind speeds, and the corresponding p_{impact}.

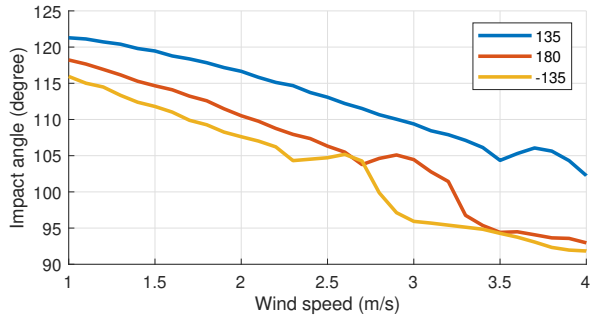

(b) Scenario 3: The three wind directions that have the biggest differences between maximum and minimum $T_{docking}$ for all wind speeds, and their corresponding ψ_{impact}.

Figure 5.27: Impact points and impact angles for the three wind directions that have the biggest time differences between maximum and minimum docking times.

Based on Figure 5.27, it can be observed that p_{impact} and ψ_{impact} are in a decreasing trend when the docking times reach their maximum values. Since the p_{impact} and ψ_{impact} decreases, the docking time should also decrease as the vessel has to slide a shorter distance, and the docking rotation is decreasing. Additionally, Figure 5.27b suggests that certain angle intervals have an effect on the $T_{docking}$. According to Table 5.5, a pattern emerges where $\psi_{impact} \in [103.8°, 115.1°]$ corresponding to the maximum $T_{docking}$. This implies that these ψ_{impact} when combined with a certain distance to the docking receiver, are suboptimal for the slide and docking rotation operations.

ψ_{impact} **for the interval with maximum** $T_{docking}$ (°)

-135°	180°	135°
114.5	114.1	115.1
113.3	113.2	114.7
112.4	112.6	113.7
111.8	111.4	113.1
111.0	110.5	112.2
109.9	109.8	111.5
109.3	108.8	110.7
108.3	107.9	110.0
107.6	107.4	109.4
107.0	106.3	108.4
106.2	105.5	107.9
104.3	103.8	107.1

Table 5.5: Scenario 2: The ψ_{impact} in the interval for highest $T_{docking}$ for -135, 180 and 135°.

According to the data presented in Table 5.6, the surge controller performs effectively for wind speeds up to 2m/s, regardless of the direction. However, for wind speeds of 3m/s, the surge controller works well in all directions except for -135°, which has been identified as the most challenging direction. In the case of wind directions of 45°and 90°, the surge controller performs well for all wind speeds. On the other hand, for the remaining tested wind directions, the surge controller experiences more difficulties at higher wind speeds.

Surge metric

Speed (m/s) \ Direction (°)	0	45	90	135	180	-135	-90	-45
0	0.179	0.179	0.179	0.179	0.179	0.179	0.179	0.179
1	0.178	0.180	0.176	0.177	0.174	0.174	0.180	0.180
2	0.176	0.173	0.167	0.162	0.165	0.169	0.177	0.188
3	0.239	0.184	0.170	0.152	0.245	0.579	0.178	0.196
4	0.285	0.135	0.130	0.360	0.668	0.598	0.203	0.210
5	0.310	0.143	0.146	0.792	0.657	0.635	0.247	0.233
6	0.325	0.187	0.159	0.744	0.673	0.493	0.308	0.298
7	0.407	0.222	0.169	0.641	0.491	0.420	0.446	0.440

Table 5.6: Scenario 2: A heatmap that shows the different surge metrics calculated for the different wind directions and speeds. The Wind direction is in degrees relative to the north. The heatmap is scaled between the maximum surge metric of 0.792, and the minimum surge metric of 0.130.

Initially, the range of the course metric spanned from 14.99 to 299.1. However, to reduce

the span, all values were divided by ten. Similar to the surge metric, the course controller demonstrates satisfactory performance for wind speeds not exceeding 2m/s. A comparison of the heatmap for the course metric with that of the surge metric reveals similarities, indicating that the course controller faces similar challenges to the surge controller with respect to certain wind directions and speeds. It is clear that the controller has problems, especially when the wind reaches speeds of 6 and 7m/s, which can indicate that the results are more based on luck than controlled docking. That the boat can slide along the pier, which gives big error margins, is the reason for successful docking rather than controlled docking.

Upon comparing the two heatmap tables, a noteworthy similarity emerges. The controller faces greater difficulties with increasing wind strength for $\beta_w = 135, 180$ and $-135°$. However, it then performs better again, leading to a red diagonal in both heatmaps. This particular observation will be subjected to further investigation in Scenario 3.

Course metric

Speed m/s \ Direction (°)	0	45	90	135	180	-135	-90	-45
0	1.499	1.499	1.499	1.499	1.499	1.499	1.499	1.499
1	3.690	3.527	2.745	2.792	4.212	4.792	3.669	2.089
2	5.244	5.760	5.883	5.594	6.628	6.825	4.680	2.688
3	7.207	7.622	7.547	8.555	6.568	18.38	5.291	2.911
4	8.344	10.47	10.25	11.17	23.82	23.01	5.893	3.427
5	9.142	13.13	12.61	29.02	24.39	20.39	6.885	4.618
6	10.26	15.26	14.57	29.91	21.96	16.37	7.616	6.728
7	13.00	15.25	17.66	14.53	10.77	9.464	8.399	12.00

Table 5.7: Scenario 2: A heatmap that shows the different course metrics calculated for the different wind directions and speeds. The Wind direction is degrees relative to the north. The heatmap is scaled between the maximum course metric of 1.499 and the minimum surge metric of 29.91. To minimize the span, all values have been divided by 10.

5.5.3 Scenario 3

In this scenario, the case that proved to be the most challenging for the docking scheme in Section 5.5.2 will be looked at.

As outlined in Section 5.5.2, it's evident that $\beta_w = -135°$poses a considerable challenge

for the docking scheme. In fact, it was when $\beta_w = -135°$that the highest p_{impact} and U_{impact} were recorded, and both the course and surge metric tables indicate that the most significant control error occurred under these conditions. As a result, the case involving $\beta_w = -135°$for stronger wind speeds will now be examined in greater detail. The first that will be looked into is the course and the desired course.

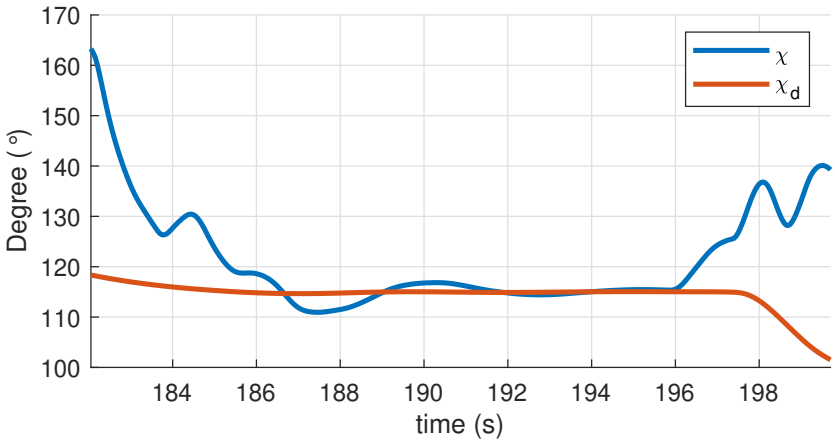

Figure 5.28: Scenario 3: The χ and χ_d plot during the approaching docking state with wind direction -135 degrees and 7m/s wind speed.

Figure 5.28 depicts the behavior of χ and χ_d during the approach docking stage. As the vessel turns, it takes some time to achieve the appropriate course, but eventually, χ becomes roughly equivalent to χ_d. However, as the vessel nears the docking receiver, the regulator struggles to maintain the desired course, resulting in significant control errors. This is logical, as U decreases when approaching the docking receiver, and the wind has a greater impact during low-speed maneuvers. During the final stages, luck plays a more prominent role in the success of the docking process, as opposed to a tightly controlled maneuver. Fortunately, the error margins are wide enough to allow for successful docking, but the operation is not entirely under full control.

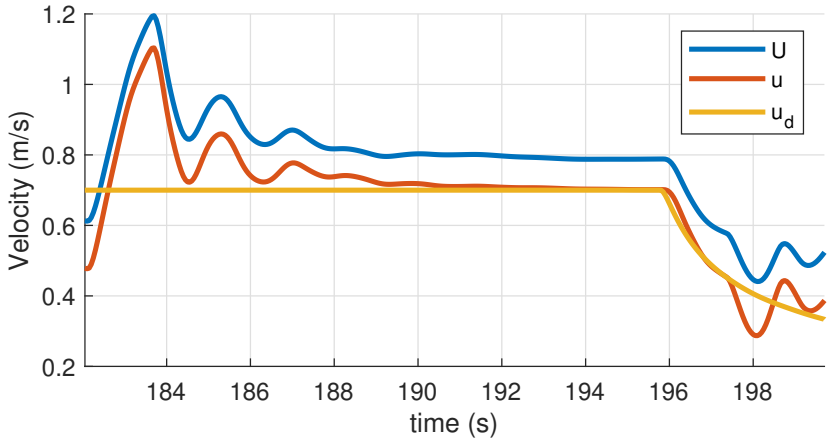

Figure 5.29: Scenario 3: The U, u, and u_d plot during the approaching docking state with wind direction -135 degrees and 7m/s wind speed.

The velocities and their corresponding desired velocities during the approach docking stage are depicted in Figure 5.29. During the transition from turning to approach docking, there is a significant disparity between u and u_d, leading to an overshoot when regulated. However, u eventually aligns with u_d. Regrettably, U is roughly 0.1 m/s higher than the u due to the lateral velocity component. Consequently, even if the surge controller regulates u appropriately, U is still too high, resulting in a high U_{impact}.

In Table 5.7, a trend shows that the controller's performance deteriorates with increasing wind strength until it suddenly improves again at 7m/s. A comparison will be made between the desired N_d and the N to understand this behavior. Since by examining this, it is possible to see if the vessel actually is helped by different wind speeds and directions and therefore gives a better result.

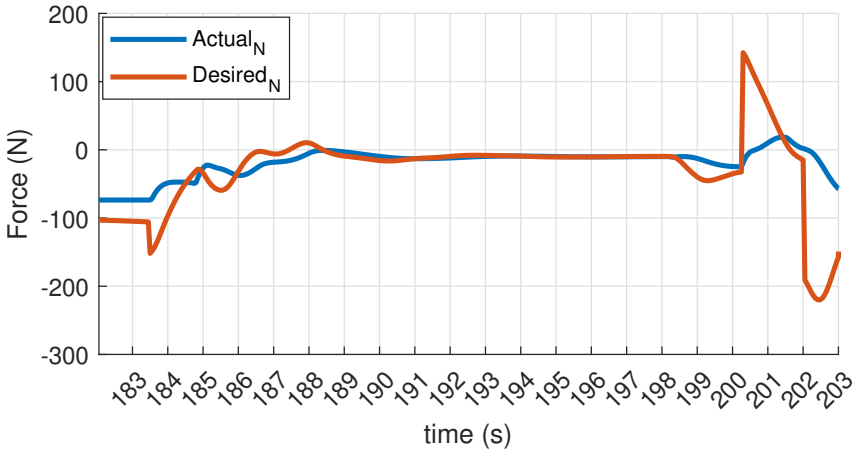

(a) Scenario 3: The desired and actual yaw moment N during the approach docking state for wind direction -135 degrees and 6m/s wind speed.

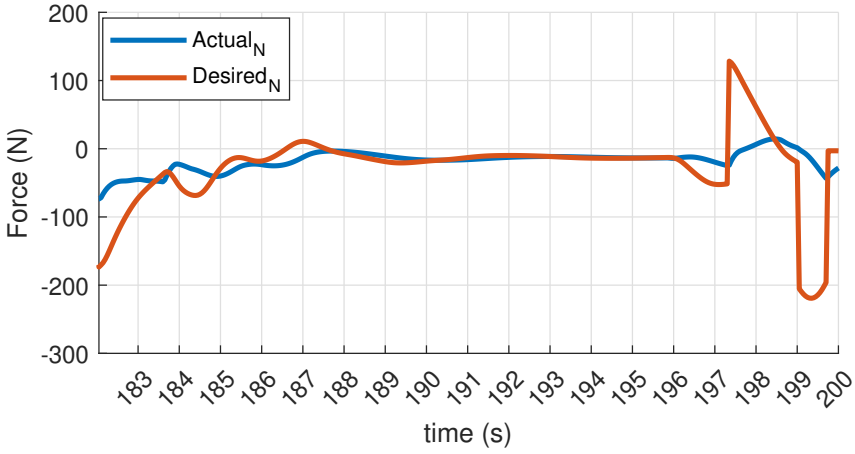

(b) Scenario 3: The desired and actual yaw moment N during the approach docking state for wind direction -135 degrees and 7m/s wind speed.

Figure 5.30: The desired and actual yaw moment N during the approach docking state.

In Figure 5.30 N_d and N are displayed in the approach docking state for $\beta_w = -135°$with 6m/s and 7m/s wind speeds. It is evident from the plot that at 6m/s, the vessel takes more time to reach the docking or pier than at 7m/s. As the metric is calculated using equation (5.1), any difference between χ and χ_d would cause an increase in the metric value at each time step in Simulink. Thus, a longer docking time leads to a higher metric value. The trend observed in the metric tables can also be attributed to the fact that the metric imposes greater penalties for distances closer to the docking receiver. As the impact point

of the vessel is further away for higher wind speeds, the metric imposes a lesser penalty, resulting in a lower value.

At a wind speed of 6m/s, $p_{impact} = 1.34$m, while $p_{impact} = 1.68$m at 7m/s. This accounts for the long time taken by the vessel to reach the pier or docking receiver as it travels a greater distance for $V_w = 6$m/s than for $V_w = 7m/s$. However, the impact point being farther away at $V_w = 7m/s$ indicates that the course controller performs even worse at that wind speed than when $V_w = 6m/s$, despite what the metric indicates. This shows that even if the metrics are a good indication of how good the controllers are, they are not completely reliable for stronger winds.

5.5.4 Scenario 4

The presented results demonstrate that the docking scheme encounters significant difficulties, particularly when $\beta_w = -135°$. The maximum p_{impact} and U_{impact} are both found to be unacceptable under these conditions. Consequently, it is necessary to modify the turning point to potentially improve the outcomes, particularly p_{impact} and U_{impact}. The original turning point [12,-12], which places the wind perpendicular to the vessel when χ is an angle of 45°. Specifically, the turning point will be relocated to $p_{turning} = [12, -6]$ to reduce the angle between the wind and the vessel's side.

The docking criteria for -135°for different turning points

Criteria	(12,-12)	(12,-6)
Impact Velocity	0.53m/s	0.36m/s
Impact Point	1.68m	0.81m
Impact to Fully docked	8.65s	5.5s
Impact Angle	97.04°	98.35°
Docking Time	36.3s	29.1s
Course Metric	9.64	29.87

Table 5.8: Scenario 4: The docking criteria for -135°for different turning points

In Table 5.8 the docking criteria for the two different turning points; $p_{turning} = [12, -12]$ and $p_{turning} = [12, -6]$ are presented. Changing the turning point results in halving the p_{impact}, which in turn directly improves the other docking criteria. The velocity reference is dependent on the distance to the docking receiver, as given (4.5). Therefore, by minimizing the $d_{docking}$ during impact, the velocity will also decrease. Additionally, the time between T_{impact} and T_{docked} will be reduced since the vessel has a shorter distance to slide as well the p_{impact} is halved. The ψ_{impact} remains close to similar for both turning points. Although the docking time is slightly decreased, it is expected as the new turning point is closer to the docking, resulting in a shorter distance to travel, and the p_{impact} is decreased. Finally, the course metric is significantly worse; however, this can be explained by the vessel being closer to docking, resulting in a higher penalty for the course metric.

5.6 Discussion

In the absence of any wind disturbance, the docking scheme operates effectively. The vessel's course and speed controllers operate smoothly and follow the references toward the docking receiver, resulting in a safe and controlled maneuver that enables the docking hitch to be securely placed into the receiver. The docking rotation ensures that the vessel is aligned with the pier, and the negative yaw moment keeps the vessel in place, allowing passengers to safely embark and disembark.

It is evident that stronger winds pose greater challenges to the safe docking of the vessel. Even if the vessel is able to dock under all tested conditions, some wind directions under strong wind conditions do not allow for completely safe docking operations. This highlights the drawback of solely focusing on surge when controlling speed. Without accounting for the total velocity, the actual velocity can be too uncertain to predict accurately. It has also been demonstrated how difficult it can be to maintain the correct course, particularly at low speeds. This can be a significant issue, as it undermines the reliability of the course controller during the critical docking phase.

Various wind directions present different challenges. When the wind pushes the vessel towards the pier, three specific wind directions cause problems with impact point and impact velocity. On the other hand, when the wind pushes the vessel away from the docking, the impact velocity and point are favorable, but the impact angle becomes significantly large for strong winds in these wind directions. In general, wind directions pointing toward the pier are the most hazardous, as higher velocities lead to more severe damage, while the other criteria are related to passenger comfort.

Varying wind directions and speeds impact the vessel's movement. To maintain the correct course, the vessel adapts its heading and surge in response to the wind. After analyzing the outcomes of Scenario 4, it is evident that adjusting the turning point leads to better results. As a result, it could be argued that the turning point should be customized for the scenario instead of using a standardized approach. This approach would be similar to how a skilled captain would approach docking a ship, taking environmental conditions, such as wind direction and speed, into consideration and adjusting the trajectory accordingly.

There are some oscillations observed in Figure 5.13 before U aligns. However, no significant improvement in tuning was accomplished during this phase. The challenge lies in regulating both the course and speed simultaneously, which becomes difficult with an underactuated vessel. This difficulty arises because both regulators utilize the same thrusters to follow their respective references.

Chapter 6

Conclusion and further work

This thesis presents the development of a complete dock-to-dock system alongside a simulator designed to test the controllers. While the docking operation is the main focus, it is worth noting that both the undocking and transit operations performed as intended, even under the strongest winds considered in this study.

Since the focus is mainly on the docking scheme, the surge and course controllers are calibrated specifically for this purpose. To improve the overall system, the transit, and undocking should have their own calibration. This can be achieved by a parameter set that tunes the controllers based on the vessel's state or by a gain schedule that tunes the controllers based on the vessel's speed.

The docking scheme functions effectively under weaker wind conditions. Specifically, where $V_w = 0$m/s, the vessel adheres to the intended course and speed, resulting in safe and controlled docking. In the average case, the docking scheme works well. However, as the wind strength increases, the controller error also increases, necessitating larger error margins for successful docking. To ensure safe and comfortable transportation for passengers during autonomous operations, it is crucial to minimize controller errors.

While the simulator used in this thesis is not calibrated with a physical system, it is deemed adequate for the intended purpose. Nonetheless, the docking routine's most challenging aspect is the docking adapters' safe connection. Although the docking rotation controller performs well in the simulator, it may require further tuning when applied to a physical system, as the accuracy of the contact forces generated by the simulator may differ from those in a real-world scenario.

The following topics have been identified as relevant for future work:

- An algorithm that decides the turning point that depends on the wind direction and wind speed. It would be reasonable for an operator to steer the vessel according to

the wind during the docking process and adjust the turning point and path accordingly.

- This thesis has not looked into efficiency, either according to time or energy; this should be looked into in further investigation of the topic.
- Bumpless transfer between the controller can be added to improve the scheme further.

Bibliography

AutoStore, 2023. The many possible uses of autostore. https://www.autostoresystem.com/insights/the-many-possible-uses-of-autostore.

Blendermann, W., 1994. Parameter identification of wind loads on ships. Journal of Wind Engineering and Industrial Aerodynamics 51, 339–351. URL: https://www.sciencedirect.com/science/article/pii/0167610594900671, doi:https://doi.org/10.1016/0167-6105(94)90067-1.

BoatUS, 2013. Docking with spring lines. https://www.boatus.com/expert-advice/expert-advice-archive/2013/february/docking-with-spring-lines.

Centre, O.A., 2023. Mapping uncharted waters more efficiently. https://oceanautonomy.no/en-us/oacnews/mapping-uncharted-waters-more-efficiently.

Ceurstemont, S., 2023. A green 'sea change' as water transport makes its move. https://ec.europa.eu/research-and-innovation/en/horizon-magazine/green-sea-change-water-transport-makes-its-move.

Fossen, T.I., 2021. Handbook of marine craft hydrodynamics and motion control.

Fossen, T.I., 2022. Marine systems simulator (mss). https://github.com/cybergalactic/MSS.

GlobalData, 2023. What are the main types of robots used in healthcare? https://www.medicaldevice-network.com/comment/what-are-the-main-types-of-robots-used-in-healthcare/.

Han, S., Wang, Y., Wang, L., He, H., 2021. Automatic berthing for an underactuated unmanned surface vehicle: A real-time motion planning approach.

Ocean Engineering 235, 13. URL: https://www.sciencedirect.com/science/article/pii/S002980182100768X, doi:https://doi.org/10.1016/j.oceaneng.2021.109352.

Haugan, I., 2023. Ntnu trials world's first urban autonomous passenger ferry. https://norwegianscitechnews.com/2022/09/ntnu-trials-worlds-first-urban-autonomous-passenger-ferry/.

Helgesen, H.H., Kristiansen, K.S., Vik, B., Johansen, T.A., 2022. Quay contact detection for ships using motion sensors and machine learning. IFAC-PapersOnLine 55, 313–319. URL: https://www.sciencedirect.com/science/article/pii/S2405896322024946, doi:https://doi.org/10.1016/j.ifacol.2022.10.448. 14th IFAC Conference on Control Applications in Marine Systems, Robotics, and Vehicles CAMS 2022.

Hendricks, J., 2012. Controlling low-speed wander. https://www.boatingmag.com/how-to/controlling-low-speed-wander/.

Horntvedt, J., 2022. Automated docking for underactuated surface vessels: A docking-adapter assisted approach. Master's thesis. Norwegian University of Science and Technology.

Hu, B., Liu, X., Jing, Q., Lyu, H., Yin, Y., 2022. Estimation of berthing state of maritime autonomous surface ships based on 3d lidar. Ocean Engineering 251, 111131. URL: https://www.sciencedirect.com/science/article/pii/S002980182200542X, doi:https://doi.org/10.1016/j.oceaneng.2022.111131.

Kockum, S., 2022. Autonomous Docking of an Unmanned Surface Vehicle using Model Predictive Contro. Master's thesis. Lund University.

Mathworks, 2022. Polynomial curve fitting. https://se.mathworks.com/help/matlab/ref/polyfit.html.

NOAA, 2023. Uncrewed surface vessels (usvs). https://oceanexplorer.noaa.gov/technology/usv/usv.html.

Optima, M., 2023. Yara birkeland. https://maritimeoptima.com/public/vessels/pages/imo:9865049/mmsi:257646000/YARA_BIRKELAND.html.

Patterson, R.G., Lawson, E., Udyawer, V., Brassington, G.B., Groom, R.A., Campbell, H.A., 2022. Uncrewed surface vessel technological diffusion depends on cross-sectoral investment in open-ocean archetypes: A systematic review of usv applications and drivers. Frontiers in Marine Science 8, 736984.

Reeco, 2023. Electronic assembly. https://www.reeco.co.uk/automation-robotics/assembly-robot/electronic-assembly/.

Robot, A., 2023. Robots in hospitals: Types, applications and advantages. https://www.agvnetwork.com/hospital-robots.

Robotics, M., 2022. The otter. https://www.maritimerobotics.com/otter.

Saab, 2022. Unmanned and autonomous. https://www.saab.com/contentassets/7bbc9bd84ccf489aa061a0dd604f15bb/unmanned_and_autonomous-220602.pdf.

Shneydor, N.A., 1998. Missile guidance and pursuit: kinematics, dynamics and control. Elsevier.

Skjetne, R., Smogeli, O., Fossen, T., 2004. Modeling, identification, and adaptive maneuvering of cybership ii: A complete design with experiments, in: IFAC Proceedings Volumes, p. 7.

SNAME, 1950. Nomenclature for Treating the Motion of a Submerged Body Through a Fluid: Report of the American Towing Tank Conference. Technical and research bulletin, Society of Naval Architects and Marine Engineers. URL: https://books.google.no/books?id=VqNFGwAACAAJ.

Strand, H.B., 2020. Autonomous Docking Control System for the Otter USV: A Machine Learning Approach. Master's thesis. NTNU.

Tech, H., 2023. Sushi restaurant deploys pudu's robotic server. https://hospitalitytech.com/sushi-restaurant-deploys-pudus-robotic-server.

Technology, S., 2023. Crewless cargo: The world's first autonomous electric cargo ship. https://www.ship-technology.com/features/crewless-cargo-the-worlds-first-autonomous-electric-cargo-ship/.

Van Amerongen, J., 1984. Adaptive steering of ships—a model reference approach. Automatica 20, 3–14. URL: https://www.sciencedirect.com/science/article/pii/0005109884900608, doi:https://doi.org/10.1016/0005-1098(84)90060-8.

Waldron, J., K., Schmiedeler, J., 2016. Kinematics. chapter 1. pp. 11–36. URL: https://doi.org/10.1007/978-3-319-32552-1_2.

Walmsness, J.E., Helgesen, H.H., Larsen, S., Kufoalor, G.K.M., Johansen, T.A., 2023. Automatic dock-to-dock control system for surface vessels using bumpless transfer. Ocean Engineering 268, 10. URL: https://www.sciencedirect.com/science/article/pii/S0029801822027081, doi:https://doi.org/10.1016/j.oceaneng.2022.113425.

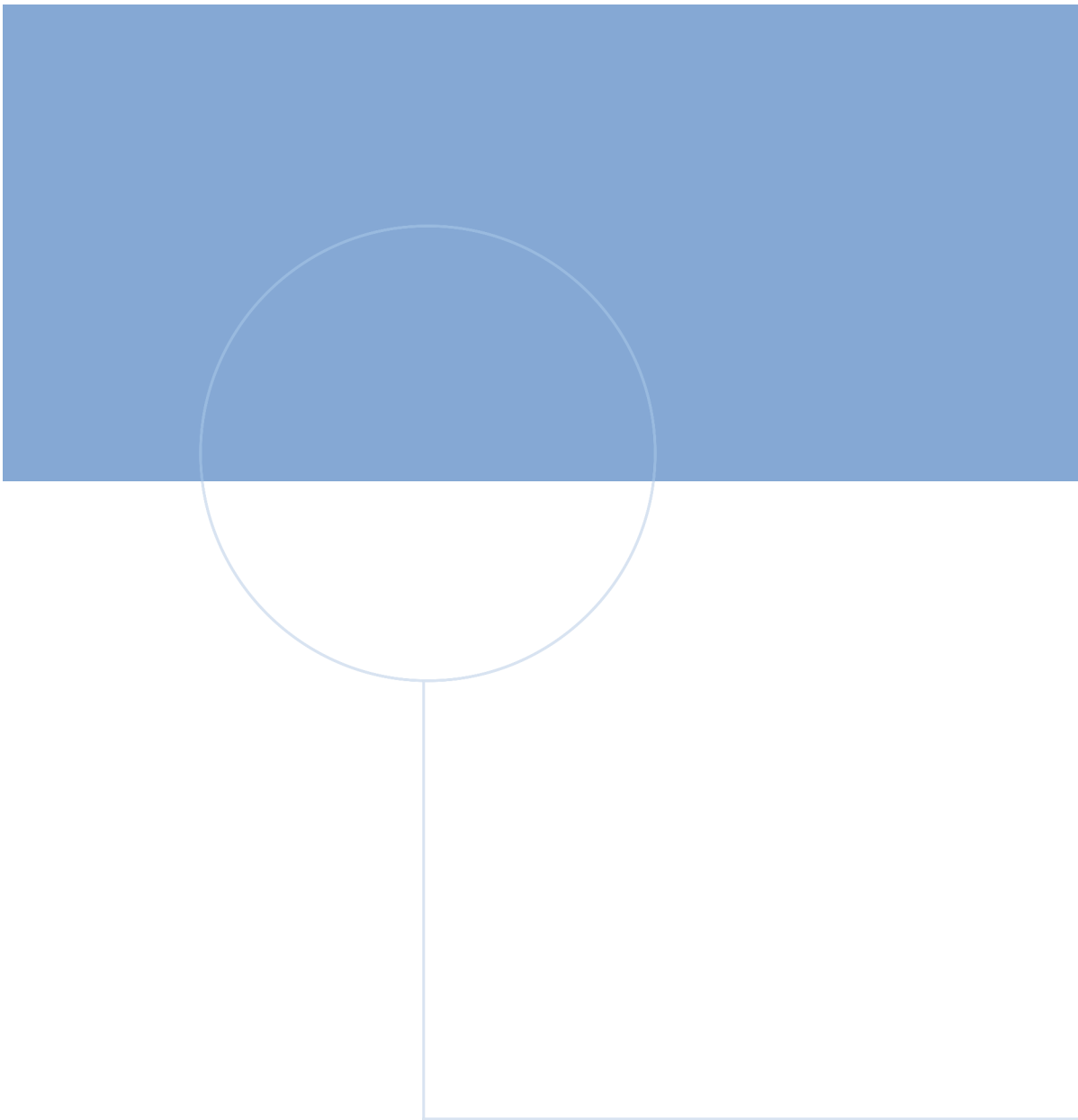

NTNU

Norwegian University of
Science and Technology